Immunohistochemical localization of MD2, a co-receptor of TLR4, in the adult mouse brain

Huazheng Liang (andyliang2018@126.com)
Tongji University https://orcid.org/0000-0001-9097-7357
Zhen Li
Tongji University
Qianyu Dong
Tongji University
Hanxi Wan
Tongji University
Xiaofei Gao
Tongji University
Lize Xiong
Tongji University

Research

Keywords: Myeloid differentiation factor 2, brain mapping, neuroinflammation, TLR4, thalamus, the red nucleus, cranial nuclei, reticular formation

Posted Date: March 15th, 2022

DOI: https://doi.org/10.21203/rs.3.rs-1432719/v1

Abstract

Background: MD2, a co-receptor of a classical proinflammatory protein TLR4 whose activation leads to neuroinflammation. It is widely accepted that TLR4 is expressed on the cell surface of microglia and astrocytes, and MD2 is expected to be expressed by these cells as well. However, our previous study showed that neurons from certain nuclei also expressed MD2. Whether MD2 is expressed by other brain nuclei is still unknown. It is the aim of the present study to map the distribution of MD2 positive cells in the adult mouse brain.

Methods: Immunohistochemical staining against MD2 was completed to localize MD2 positive cells in the mouse brain by comparing the location of positive cells with the mouse brain atlas. Retrograde tracing and double immunofluorescence staining with both MD2 and TH were conducted to examine whether dopaminergic neurons in the substantia nigra projecting to the striatum were MD2 positive.

Results: MD2 positive cells were found in the majority of mouse brain nuclei with clusters of cells in the olfactory bulb, cortices, the red nucleus, and cranial nuclei. Subcortical nuclei had heterogenous staining of MD2 with more prominent cells in the basolateral and the central amygdaloid nuclei. The ventral pallidum and the diagonal bands had positive cells with similar density and shape. Prominent cells were present in thalamic nuclei which were nearly homogenous, reticular formation of the brainstem where cells were dispersed with similar density. The hypothalamus had fewer outstanding cells compared with the thalamus. The red nucleus, the substantia nigra, and the ventral tegmental area in the pretectum had outstanding cells with the latter two containing dopaminergic neurons projecting to the striatum as shown in retrograde tracing and double fluorescence staining. Raphe, sensory cranial, and deep cerebellar nuclei also had MD2 positive cells with moderate density.

Conclusion: MD2 is present not only in glial cells, but also in neurons. Some MD2 positive dopaminergic neurons in SNC and VTA projected to the striatum.

Introduction

Myeloid differentiation factor 2 (MD2) is classically known as the co-receptor of the Toll-like receptor 4 (TLR4) signaling pathway. They are the key elements of lipopolysaccharide (LPS) induced neuroinflammation [1, 2]. LPS, once bound to MD2 in the presence of lipopolysaccharide binding protein (LBP) and cluster of differentiation 14 (CD14) [3], triggers dimerization of the TLR4-MD2-LPS complex [4], which activates two intracellular signaling pathways, the myeloid differentiation primary response 88 (MyD88) and Toll-interleukin-1 receptor domain-containing adapter inducing interferon-β (TRIF) [5–7]. A variety of proinflammatory cytokines are produced and released [2, 8–11] as a result of the activation of downstream proteins (MyD88 dependent and independent pathways) [6, 7] and translocation of transcription factors including transforming growth factor β-activated kinase 1 (TAK1) [5, 12], mitogen-activated protein kinases (MAPKs) [5], nuclear factor k-B (NF-kB), activator protein-1 (AP-1), cAMP response element binding protein (CREB) [2, 13]. Consequently, these toxic substances lead to neuronal

injury or cell death [14–17], even depression or cognitive impairment [1, 2, 8]. This phenomenon is not only observed in the nervous system but also other types of tissue, such as the heart [2, 18].

Due to the importance of MD2 and TLR4 in the pathogenesis of a number of neurological conditions which manifest with neuroinflammation [19, 20], many drugs have been developed to suppress neuroinflammation with an aim to protect neurons or ameliorate neuronal injury. It is widely known that microglia cells and astrocytes are the dominant endogenous cells that are involved in neuroinflammation. Studies have focused on impact of these two types of cells in inflammatory conditions. TLR4 is present in both microglia and astrocytes and it is expected that its co-receptor MD2 is also present on the membrane of these cells. Previously, it has been reported that TLR4-MD2 is primarily expressed by microglia [21], and also expressed by astrocytes [22], neurons [23], oligodendrocytes [24], and endothelial cells in the central nervous system, suggesting that activation of TLR4-MD2 might induce neuronal injury by bypassing glial cells.

For LPS to bind TLR4, LBP and CD14 are required. Binding of LPS to LBP enables this complex to attach to CD14. The latter, a glycolipid-anchored membrane protein on innate immune cells, mediates the interaction of LPS with MD2 [25, 26]. This suggests that the classical LPS-TLR4-MD2 signaling pathway can only be found on immune cells or requires the participation of immune cells if MD2 is expressed on neurons. Surprisingly, we found that MD2 was also expressed by neurons in our previous study, and to a lesser extent by microglia or astrocytes [27]. This paradoxical phenomenon has led to our comprehensive mapping of MD2 in the central nervous system using immunohistochemical staining. To our surprise, MD2 was indeed predominantly present on the membrane of neurons. Herein, we present the detailed mapping results on neurons.

Materials And Methods

Animals and grouping

C57BL/6 mice of 12-14 weeks of age, weighing 25-30 g were used and obtained from Beijing Vital River Laboratory Animal Technology Co., Ltd. Rats were housed in standard breeding cages and maintained on a12-h light/dark cycle at 21±2℃ with food and water ad libitum. All procedures were approved by the Animal Research Ethics Committee of Tongji University (approval number TJBH00421401).

Retrograde tracing

Mice were anesthetized using 1.5% isoflurane as described above. After removing the fur on the head, the mouse skin was defected with 75% ethanol. A longitudinal incision was made on the skin to expose the skull. Stereotaxic coordinates were confirmed with the assistance of the Mouse Brain in Stereotaxic Coordinates and 60 nl of Fluoro-gold was injected into the striatum (Bregma: 1.42-0.02 mm; midline: 1.25-3.00 mm; dorsoventral: 1.25-3.75 mm) using a Hamilton syringe within 10 min. After leaving the needle in

situ for 10 min, the needle was slowly withdrawn. The skull was sealed with bone wax and the skin sutured. Topical analgesic was applied to the incision area.

Tissue preparation

After completing behavioral tests, mice were anesthetized with 1.5% isoflurane again. The skin over the chest and the upper abdomen was incised and the heart was exposed after cutting the diaphragm. A 23G needle connected to a peristaltic pump was inserted into the left ventricle and an incision was made on the right atrium. Mice were then flushed with 0.9 % normal saline, followed by 50 ml of 4 % paraformaldehyde (Sinopharm, dissolved in 1x PBS). The mouse brain was removed and postfixed in 4 % paraformaldehyde for 2 hours at 4 °C, and then transferred to 30% sucrose (dissolved in 1x PBS). After the brain sank to the bottom of the container, it was cut into 40 μm thick sections using a Leica CM 1950 cryostat. Every sixth section from the brain was used for immunohistochemical staining.

Immunohistochemical/immunofluorescence staining

Immunohistochemical staining for myeloid differentiation factor 2 (MD2) was undertaken on every sixth of the brain sections of four mice in each group. Sections were washed after cutting and treated with 1 % H_2O_2 in 50 % ethanol to quench endogenous peroxidases. Section were then transferred into 5 % goat serum in 1x PBS to block non-specific antigen binding sites. They were incubated in the primary anti-MD2 (rabbit, 1:1000, GTX85517, GeneTex) solution overnight and subsequently in the secondary antibody (Biotin-SP AffiniPure donkey anti-rabbit IgG (H+L), 1:500, 711-065-152, Jackson Immunoresearch Laboratories) for 2 h. Sections were then washed and transferred to an extravidin peroxidase solution (Sigma, 1:1000) for 2 h. Finally, the sections were incubated in a 3,3-diaminobenzidine (DAB) reaction complex (Vector lab, Burlingame, CA, USA) until an optimal colour developed. At the end of the procedure, the sections were mounted and dehydrated in gradient ethanol and cleared in xylene before being coverslipped.

For immunofluorescence staining, sections from FG-injected mice were washed and incubated in 5 % goat serum in 1x PBS to block non-specific sites. After 2 h, sections were incubated in the MD2 antibody (1:200, GTX85121-mouse, GeneTex) and tryrosine hydroxylase (1:500, AB152-rabbit, Millipore) solution f or overnight. After 3 rinses, sections were incubated in Cy3 conjugated donkey anti-rabbit IgG (H+L) and Cy5 conjugated donkey anti-mouse IgG (H+L) solution for 2 h at room temperature. Finally, sections were washed and mounted onto slides, followed by coverslipping with a fluorescent mounting medium.

Data analysis

Mouse brain sections were scanned with a 3D Histech Pannoramic digital scanning system at 20x magnification. High resolution scanned images of the brain were then compared with diagrams of the

mouse brain from “The Mouse Brain in Stereotaxic Coordinates” [28]. Distribution of MD2 positive neurons were then mapped.

Results

Olfactory nucleus

MD2 positive cells were observed along the longitudinal axis of the mouse brain. In the olfactory bulb, positive cells were dominantly found in the dorsal (AOD) (**Fig 1A**), lateral (AOL) (**Fig 1B**), and the lateral part of the ventral olfactory area (AOV) (**Fig 1C**), followed by positive cells in the medial olfactory area (AOM) (**Fig 1D**) and cells in the mitral cell layer rostrally (**Fig 1E**). Few cells were found in the external plexiform layer of the olfactory nucleus and the rest of this nucleus. Positive cells were also in the posterior part of the olfactory area (AOP) caudally (**Fig 1F**). Laterally, there were positive cells in the piriform cortex (Pir) (**Fig 1G**) as those in the lateral part of the olfactory area. Medially, there were positive cells in both the dorsal (DTT) and ventral tenia tecta (VTT) (**Fig 1H**).

Cerebral cortex

MD2 positive cells were found nearly in all cortical regions. Rostrally, positive cells were predominantly found in the frontal association area (FrA) (**Fig 2A**), the medial (MO) (**Fig 2B**), ventral (VO), lateral (LO) (**Fig 2C**), and ventrolateral orbital cortex (VLO) with fewer positive cells in layer 4. Few positive cells were found in the superficial layers (1-2). In the primary (M1) (**Fig 2D**) and secondary motor cortex (M2), primary sensory cortex (S1) (**Fig 2E**), area 3 of the frontal cortex, dysgranular insular cortex (DI), there was a band of weakly labelled cells in the superficial layers from layer 1 to layer 3. More caudally, strongly labeled cells concentrated in layer 4 in these brain regions. Similar phenomenon was also observed in Pir, the visual (V1), and the auditory cortex (Au1). In the dorsal (AID) and ventral (AIV) parts of the agranular insular cortex, the superficial layers were nearly void of positive cells in their rostral portion (**Fig 2F**). But this was not applied to the more caudal portion of them. At the same level, the dorsal peduncular cortex (DP) (**Fig 2G**), the infralimbic (IL) (**Fig 2H**) and the prelimbic (PrL) cortices did not have such a band void of positive cells. In the caudal brain regions such as the dorsolateral entorhinal cortex (DLEnt) (**Fig 3A**) and the perirhinal cortex (PRh) (**Fig 3B**), more prominent cells were found in the entire depth of the cortex except layer 1 and 2. In the hippocampus, clustered positive cells were observed in the pyramidal cell layer (**Fig 3C**), whereas scattered positive cells were found in other layers of the hippocampus. Among CA1-3, CA2 (**Fig 3D**) and CA3 (**Fig 3E, F**) seemed to have more prominent staining than CA1. The dentate gyrus (DG) had very weakly labeled cells in the granule cell layer and scattered cells in other layers (**Fig 3E**). In the caudal part of the hippocampus, MD2 positive cells were found in the dorsal subiculum (DS) (**Fig 3G**) as well. CA2 had more positive cells throughout its layers except the deeper layers. Positive cells were observed in both the auditory (**Fig 3I**) and visual cortex (**Fig 3J**) with more prominently labeled cells in layer 5 and 6.

Subcortical nuclei

In the accumbens, neither the core (AcbC) (**Fig 4A**) nor the shell (AcbSh) (**Fig 4B**) had strongly labeled cells. Instead, they had weakly labeled cells throughout the nucleus. Ventrally, a small number of strongly labeled cells were found in the ventral pallidum (VP), especially in the lateral part (**Fig 4C**). There were more strongly labeled cells in its caudal part, rendering a continuous band of cells with those in the horizontal diagonal band (HDB) (**Fig 4D**). Only weakly labeled cells were found in the olfactory tubercle (Tu) with a band void of cells ventral to those strongly labeled cells (**Fig 4E**). The major island of Calleja (ICj) was nearly void of positive cells. In the septum, positive cells were found in the dorsal (LSD) (**Fig 4F**), ventral (LSV) and the intermediate parts (LSI) of the lateral septum (**Fig 4G**). In the rostral medial septum (MS), a small number of strongly labeled cells were found intermingled with other positive cells. There were more strongly labeled cells in the caudal part of the medial septum (**Fig 4G**) as well as in the vertical (VDB) and horizontal diagonal bands (HDB) (**Fig 4H**). In the caudate putamen (CPu), positive cells were sparsely distributed throughout these nuclei (**Fig 4I**). Labeled cells were found in both the dorsal (DCl) and ventral claustrum (VCl), especially in the ventral part (**Fig 4J**). In contrast, much fewer positive cells were observed in the dorsal (DEn) and the intermediate endopiriform claustrum (IEn) as well as the lateral stripe of the striatum. At the level of fused anterior commissure, strongly labeled cells extended laterally from the horizontal diagonal band to the anterior amygdaloid area (AA) (**Fig 5A**), especially its dorsal part. Ventral to the posterior limb of the anterior commissure, a small number of weakly labeled cells were found in the interstitial nucleus of the posterior limb of the anterior commissure (IPAC). More caudally, positive cells were also found in the globus pallidus (GP) with a higher density of cells than in the CPu (**Fig 5B**), which was similar to that of the anterior (BLA) and posterior basolateral amygdaloid nucleus (BLP) (**Fig 5C**), and the posterior part of the basomedial amygdaloid nucleus (BMA) where positive cells were even more packed than those cells in layer 4 of the cortex (**Fig 5D**). The central amygdaloid nucleus, especially the medial division (CeM) had similarly labeled cells (**Fig 5E**). Positive cells in other amygdaloid nuclei ventral to the basolateral amygdaloid nucleus were less prominent. Positive cells in layer 2 of the posterolateral cortical amygdaloid nucleus (PLCO) were packed like those in the piriform cortex (**Fig 5F**).

Hypothalamus

Rostrally, few MD2 positive cells were found in both the lateral (LPO) (**Fig 6A**) and the medial preoptic areas (MPA) (**Fig 6B**), the basal part of the substantia innominate (SIB) (**Fig 6C**) where positive cells were similar to those in the HDB, and more patches of cells in the bed nucleus of the stria terminalis (STM) (**Fig 6D**). Next to the 3rd ventricle, positive cells were observed in the anteroventral periventricular nucleus (AVPe) (**Fig 6E**), ventromedial preoptic nucleus (VMPO), median preoptic nucleus (MnPO). At the level of anterior commissure decussation, a small number of positively labeled cells were observed in the above nuclei with few cells in the medial preoptic area (MPA). More caudally, more positive cells were observed in the medial preoptic nucleus (MPO) (**Fig 6F**), and to a lesser extent in the MPA, the lateral preoptic nucleus (LPO), the anterior hypothalamic area (AHA) which is more lateral to MPO (**Fig 6G**). Caudal to

AHA, positive cells were also present in the central (AHC) and posterior parts (AHP) of the anterior hypothalamic areas (**Fig 6H**) which had a small number of more prominent cells similar to those found in the lateral hypothalamus (LH) (**Fig 7A**). Medially, the ventromedial hypothalamic nucleus (VMH) had a small number of positive cells (**Fig 7B**) in contrast to the dorsomedial hypothalamic nucleus (DM). Dorsolaterally, positive cells were also seen in the zona incerta, especially in the lateral part (ZI) (**Fig 7C**) where it is approaches positive neurons in the entopedunclular nucleus (EP) (**Fig 7D**). Dorsally, positive cells were also found in the anterior parvicellular part (PaAP) (**Fig 7E**), the medial parvicellular part (PaMP), the medial magnocellular part (PaMM) (**Fig 7E**), and the posterior paraventricular hypothalamic nucleus (PaPo) (**Fig 7F**) and they were less prominent than those in the lateral hypothalamus. Positive cells were present in the lateral hypothalamic area (LH) and they were nearly continuous with those cells in the entopeduncular nucleus (EP), especially in peduncular part of the lateral hypothalamus (PLH) (**Fig 7G**) where a small number of large cells were present in the magnocellular nucleus of the lateral hypothalamus (MCLH) (**Fig 7H**).

Thalamus

In the thalamus, the most prominent nucleus is the anterodorsal thalamic nucleus (AD) (**Fig 8A**) which had the highest density of positive cells, followed by the reticular nucleus (Rt) (**Fig 8B**), the ventral posterolateral thalamic nucleus (VPL) (**Fig 8C**), the ventrolateral thalamic nucleus (VL) (**Fig 8D**), the ventromedial thalamic nucleus (VM) (**Fig 8E**), and the reuniens thalamic nucleus (Re) (**Fig 8F**). More caudally, positive cells were observed in the dorsomedial part of the laterodorsal thalamic nucleus (LDDM) (**Fig 8G**). The density of positive cells was similar to that of the ventrolateral thalamic nucleus. Positive cells were evenly distributed in the anteroventral thalamic nucleus (AV), the anteromedial thalamic nucleus (AM), and the pericentral (PC) as well as the central medial thalamic nuclei (**Fig 8H**). At the level when fasciculus retroflexus (fr) emerged, densely packed cells were observed in the subthalamic nucleus (STh) (**Fig 9A**), and to a lesser extent in the dorsal lateral geniculate nucleus (DLG) (**Fig 9B**), the medial geniculate (MG) (**Fig 9C**), as well as in the parafascicular thalamic nucleus (PF) (**Fig 9D**). Moderately labeled cells were also observed in other thalamic nuclei.

Pretectum

In the pretectum, clusters of positive cells were observed in the lithoid nucleus (Lth) and adjacent retroparafascicular nucleus (RPF) which is more lateral than the lithoid nucleus (**Fig 9E**). Fewer positive cells were found in other regions at the level of the rostral commissure except a small number of positive neurons in the nucleus of the optic tract (OT) (**Fig 9F**). Ventrally, positive cells were seen in the nucleus of Darkschewitsch (Dk) (**Fig 9E**) and to a lesser extent in the interstitial nucleus of Cajal (InC), the pre-Edinger Westphal nucleus (PrEW) (**Fig 9G**), and in the reticular formation of prosomere 1 (p1Rt). A small number of positive cells were also observed in the magnocellular nucleus of the posterior commissure (MCPC) (**Fig 9H**). More ventrally, positive neurons were present in the compact (SNC) (**Fig 9I**) and reticular

(SNR) parts of the substantia nigra (**Fig 9K**), the adjacent parasubthalamic nucleus (PSTh) (**Fig 9I**), the rostral part of the ventral tegmental area (VTA) (**Fig 9J**) and the region between this and the fasciculus retroflexus (fr) where a small number of positive cells were found in the Forel field (F) and the prerubral field (PR) (**Fig 9L**). Sparsely labeled cells were also observed in the anterior pretectal nucleus (APT) and other nuclei in the pretectum.

Brainstem

In the rostral midbrain, positive cells were present in the entire superior colliculus (SC), with prominent cells in the lateral portion of the intermediate (InG) and deep gray layers of this nucleus (DpG) (**Fig 10A**). Positive cells in the mesencephalic reticular formation (mRt) (**Fig 10B**) were less outstanding than those in the magnocellular part of the red nucleus (RMC) (**Fig 10C**), but more prominent than those in the periaqueductal gray (PAG) (**Fig 10D**). Fewer positive cells were seen in the region between the interpeduncular nucleus (IP) which had sparsely labeled cells (**Fig 10E**), and RMC (**Fig 10F**). At the caudal level of the RMC, a cluster of positive cells were found in the oculomotor nucleus (3N) (**Fig 10G**). Lateral to IP, a small number of cells were also found in the region between SNC and IP. There was an increasing number of positive cells in the SNR of the midbrain. Caudal to cells in 3N, a small cluster of cells were also observed in the trochlear nucleus (4N) (**Fig 10H**). Ventral to the superior colliculus, sparsely labeled cells were found in the inferior colliculus (IC) and in the region lateral to PAG, corresponding to the precuneiform nucleus (PrCnF) (**Fig 10I**).

In the rostral pons, positive cells were predominantly found in the pontine nuclei (Pn) (**Fig 10J**), the reticular tegmental nucleus, median raphe nucleus (MnR) (**Fig 10K**), and the ventral nucleus of the lateral lemniscus (VLL) as well as the paralemniscal nucleus (PL) (**Fig 10L**). Adjacent to the MnR, scattered positive cells were observed in the oral pontine reticular nucleus (PnO) (**Fig 10L**). There were few cells between PnO and PL. At the level of the trochlear nucleus, a small cluster of positive cells were found in the parabigeminal nucleus (PBG) (**Fig 11A**). At the caudal end of this nucleus, positive cells were also observed in the dorsal and intermediate nuclei of the lateral lemniscus. At the level of the rostral end of the motor trigeminal nucleus (5N) (**Fig 11B**), a cluster of strongly labeled cells were found in the trapezoid nucleus (Tz), and to a lesser extent in the central nucleus of the acoustic tract (CAT) (**Fig 11C**) and adjacent medioventral periolivary nucleus (MVPO) and paraolivary nucleus. MD2 positive cells were found in 5N throughout its rostrocaudal axis with a similar density of cells to that of reticulotegmental nucleus of the pons (RtTg) (**Fig 10L**). Medial to 5N, positive cells were found in the subcoeruleus nucleus (SubC) whose positive cells were less prominent than those in 5N (**Fig 11D**). In contrast, the principal sensory trigeminal nucleus (Pr5) had a lower density of positive cells and the majority of cells were in the dorsal medial part of this nucleus (Pr5DM) (**Fig 11B**). Tegmental nuclei dorsal to the medial longitudinal fasciculus (mlf) had few positive cells, whereas the caudal pontine nucleus, which is ventral and medial to mlf, had a small number of outstanding cells (**Fig 11E**).

At the level of the genu of the facial nerve (g7), prominent positive cells were observed in the facial nucleus (7N) including the stylohyoid part (7SH) (**Fig 11F**), the anterior part of the ventral cochlear nucleus (VCA) (**Fig 11G**), the abducens nucleus (6N) (**Fig 11H**). A small number of strongly labeled cells were present in the locus coeruleus (LC) and less prominent cells in the Barrington nucleus (Bar) (**Fig 11I**). Few weakly labeled cells were observed in the parabrachial nuclei (MPB, LPB) (**Fig 11J**) except the internal part of the lateral parabrachial nucleus (LPBI). From Bar towards the midline, there was a decreasing gradient of positive cells in the dorsal part of the hindbrain including the latero- (LDTg) and posterodorsal tegmental nuclei (PDTg). Ventral to the facial genu, there were positive cells in the principal trigeminal nucleus (Pr5) with a relatively low density compared to positive cells in the adjacent reticular formation. A small number of positive cells were observed in the oral part of the spinal trigeminal nucleus (Sp5O) (**Fig 11K**). In more caudal parts of this nucleus including the interpolar and the caudal Sp5, there was an increasing gradient of cell density. Medial to Pr5 and Sp5, positive cells were present in the parvicellular (PCRt) and intermediate reticular nuclei (IRt) (**Fig 11L**) as well as the caudal pontine reticular nucleus (PnC) rostrally and gigantocellular reticular nucleus (Gi) caudally (**Fig 11F**) with a relatively higher density in its ventral portion. Relatively fewer positive cells were present in the dorsal paragigantocellular nucleus (DPGi) (**Fig 12A**). Along the midline, positive cells were also observed in both the raphe magnus nucleus (RMg) and the raphe pallidus nucleus (RPa) (**Fig 12B**). MD2 was strongly expressed by Purkinje cells in the cerebellum (**Fig 12C**), but not by other cells except some cells in lobule 9 of the cerebellar vermis (9Cb). Interestingly, all cerebellar nuclei had MD2 positive cells, including the interposed (IntA, IntP) (**Fig 12D**), the lateral cerebellar nuclei (Lat) (**Fig 12E**), the medial (Med) (**Fig 12F**), and the vestibulocerebellar nucleus (VeCb) (**Fig 12G**). In the vestibular complex, positive cells were observed in all nuclei. Those in the superior (SuVe) (**Fig 12H**), lateral (LVe) (**Fig 12I**), spinal vestibular nuclei (SpVe) (**Fig 12K**) were evenly distributed and segregated by fibers travelling in these nuclei. The medial vestibular nucleus (MVe) demonstrated a different feature from other vestibular nuclei. It had fewer positive cells than the adjacent LVe (**Fig 12J**), which was similar to that of the rostral prepositus nucleus (Pr). The caudal Pr had relatively more positive cells than the rostral counterpart (**Fig 12L**). In the caudal part of IRt, a small cluster of positive cells were observed in the ambiguus nucleus (Amb). The adjacent linear nucleus (Li) also had positive cells in its lateral and dorsal limbs, reflecting its inversed L shape (**Fig 13A**). The lateral reticular nucleus (LRt) were continuous with Li and it had positive cells dispersed in the entire nucleus (**Fig 13B**). At the level of the hypoglossal nucleus (12N), positive cells were observed in this nucleus and the adjacent vagus nerve nucleus (10N) (**Fig 13C**). Laterally, positive cells were observed in the interpolar part of the spinal trigeminal nucleus (Sp5I) (**Fig 13D**), which were more prominent than those in the rostral counterparts. More dorsolaterally, positive cells were found in the external cuneate nucleus (ECu) (**Fig 13E**), and to a lesser degree in the cuneate nucleus (Cu), especially in the caudal end of this nucleus. Ventrally, weakly positive cells were present in the inferior olive (IO) (**Fig 13F**). This nucleus, along with ECu, LRt, and Li, is known to project to the cerebellum. In the caudal end of the medulla, positive cells were present in both the dorsal (MdD) (**Fig 13G**) and ventral medullary reticular nuclei (MdV) (**Fig 13H**) with more strongly labeled cells in MdV.

After injecting FG to the caudate and putamen, FG labeled cells were found in both the substantia nigra, especially in the compact part, and the ventral tegmental area (**Fig 14A**). FG labeled cells in these two nuclei were almost continuous with each other with more labeled cells in the VTA, forming a cluster of cells. TH staining showed a large number of positive cells in these two nuclei, especially in VTA (**Fig 14B**) and they were overlapping with FG labeled neurons. MD2 staining showed that positive cells (**Fig 14C**) are overlapping with TH positive and FG labeled cells to a great extent (**Fig 14D**), indicating that MD2 positive cells are mainly CPu projecting dopaminergic neurons.

Discussion

To our knowledge, the present study is the first to systematically map the distribution of MD2 positive cells in the mouse brain. We found that MD2 was present in the majority of mouse brain nuclei, especially in the olfactory bulb, motor and sensory cortices, the thalamus, the red nucleus, cranial motor nuclei and the reticular formation. Subcortical nuclei had MD2 positive cells with different density and staining intensity. Prominent cells were found in the basolateral and the central amygdaloid nuclei, the ventral pallidum and the diagonal bands. The thalamus had nearly homogenous MD2 positive cells in the majority of thalamic nuclei. The hypothalamus had fewer outstanding cells compared with the thalamus. The red nucleus, the substantia nigra, and the ventral tegmental area in the pretectum had outstanding cells. Retrograde tracing and double fluorescence staining showed that the substantia nigra and ventral tegmental area contained dopaminergic neurons projecting to the striatum. The raphe, sensory cranial, deep cerebellar nuclei, and reticular formation of the brainstem had dispersed MD2 positive cells with moderate density.

Previously, MD2 was thought to be expressed mainly by microglia in the central nervous system. However, studies by Fang et al have shown that MD2 was also positive in cortical neurons, and the expression in neurons was enhanced by NMDA stimulation or stroke-induced injury [27]. When microglia cells were depleted by PLX3397, cerebral ischemia/reperfusion injury still increased the expression of MD2 [27], suggesting that microglia were not the only type of cells that express MD2. Our results are consistent with theirs in that MD2 was positive in brain regions, such as the ventral pallidum, rostral medial septum, anterior amygdaloid area, globus pallidum, anterodorsal thalamic nucleus, subthalamic nucleus, pontine nuclei, reticular tegmental nucleus, trapezoid nucleus, and the locus coeruleus. Kunda et al. also reported that MD2 was not exclusively expressed in microglia, and labeled cells were also present in neonatal trigeminal and nodose neurons [29]. It is well accepted that the LPS/TLR4/MD2 signaling pathway is involved in innate immune responses. Interestingly, Kunda et al. [29] demonstrated that LPS stimulation resulted in downregulation of MD2 mRNA in neonatal trigeminal and nodular neurons, suggesting that LPS also takes effect in trigeminal neurons and nodular neurons through its typical receptors like in microglia. Our research adds more evidence to the results of Kunda et al. by showing that MD2 was positive in motor trigeminal nucleus. Zuo et al. [30] noted that MD2 was prominently expressed in neurons in the hippocampus of aged mice, while a small amount of MD2 was still positive in microglia. Our results are also consistent with their findings regarding the presence of MD2-labeled neurons in the hippocampus. In the hippocampus, clustered positive cells were observed in the pyramidal cell layer. In

addition, we found that MD2-labeled cells were positive in brain regions such as the oculomotor, facial, the ventral cochlear, the abducens, the red, and the motor trigeminal nuclei.

It is generally accepted that MD2 and TLR4 are mainly present in microglia, and TLR4-MD2 signaling pathway is a crucial one in innate immune and inflammatory response. Upon exposure to endotoxins, such as LPS, glia cells like microglia and astrocytes could elicit neuronal injury or necrosis through the TLR4-MD2 signaling pathway. As a key component, MD2 recognizes and initiates the innate immune response to bacterial LPS [31]. It is anchored to TLR4 on the membrane and binds to LPS, mediating the transduction of the incoming LPS signal. Once the binding completes, dimerization of the complex occurs. In addition to the classical TLR4-MD2 signaling pathway, Fang et al. demonstrated that MD2 induced neuronal apoptosis and necroptosis in a rodent stroke model through a TLR4-independent, SRC associated in mitosis of 68kDa (Sam68)-related cascades. They found that the expression of MD2 was increased one hour after NMDA stimulation and this lasted for 12 hours. However, the expression of TLR4 was not synchronous with that of MD2. Its expression was not enhanced until four hours after NMDA stimulation and its pattern was different from that of MD2. Surprisingly, the expression of MD2 was still significantly increased in TLR4 knockout mice. These results suggest that MD2-mediated neuronal injury may not be fully dependent on TLR4 activation. Surface plasmon resonance (SPR) experiment has shown that MD2 may induce neuronal injury by interacting with Sam68. Dissociating MD2 from Sam68 protected neurons in cultured neurons where TLR4 was knocked out.

Zuo et al. [30] also reported that MD2 played an important role in the pathogenesis of perioperative neurocognitive disorder (PND). They demonstrated that anesthesia and surgery impaired spatial learning and memory of aged mice, and increased the expression of MD2. Knockout of MD2 or administration of MD2-degrading peptide Tat-CIRP-CMA could ameliorate cognitive impairment [30]. In addition, down-regulating MD2 resulted in decreased level of α5GABA$_A$R and its tension current, whereas activating α5GABA$_A$R curtailed the therapeutic effect of Tat-CIRP-CMA, suggesting that MD2 is involved in the pathogenesis of perioperative neurocognitive dysfunction by increasing the expression of α5GABA$_A$R and its tension current in aged mice[30]. Apart from the abovementioned mechanisms of MD2-mediated neuronal injury in stroke and neurocognitive disorders, MD2 is able to elicit neuronal injury and inflammation through the classical TLR4-MD2 signaling pathway. Activation of this pathway in rodents results in not only neuroinflammation, but also neurobehavioral disorders such as depression which contributes to the pathology of Alzheimer's disease [32]. Therefore, inhibiting MD2 activity is a potential therapeutic strategy for the management of inflammation-related brain injury or other vital organ lesions.

Currently, a number of drugs have been developed to target MD2. MD2 antagonists could be used to treat many systematic diseases including neuroinflammation [33–38], focal cerebral ischemia [39, 40], sepsis [41, 42], nephropathy caused by obesity [43], osteoarthritis [44], inflammation caused by acute lung injury[45–47] and neuropathic pain [18]. The majority of MD2 antagonists/inhibitors take effect through interacting with functional domains of MD2. For example, a few compounds target the hydrophobic binding pocket of MD2, such as eritoran, (+)-norbinaltorphimine, ITH12674, lovastatin, rifampin, ciprofloxacin, curcumin, and GG6. This interaction with the hydrophobic binding pocket of MD2 prevents

the stabilization of LPS. In contrast, other compounds target the interface between MD2 and TLR4, such as ferulic acid[8] and Fast Green FCF [48]. Ferulic acid interrupts the steady state of the TLR4-MD2 complex by competitively binding to TLR4, whereas Fast Green FCF prevents the formation of TLR4-MD2 complex through anchoring to TLR4 with the assistance of the hydrogen bond formed with TLR4 residues. More interestingly, Fang et al[27] developed a small peptide named Tat-CIRP which interrupted the stabilization of the TLR4-MD2 complex by competitively binding to MD2, and effectively reduced neuronal apoptosis and necroptosis, leading to strong and sustained neuroprotection in rodent and primate stroke models. Zuo et al. [30] synthesized a similar peptide, Tat-CIRP-CMA, which can cross the blood-brain barrier and degrade MD2. This consequently ameliorated cognitive impairment of aged mice undergoing anesthesia and surgery [30]. However, few MD2 antagonists or inhibitors which show therapeutic effects in both in vivo and in vitro studies have been translated into medications for clinical use. Future investigations are needed to reveal the underlying mechanism.

In the present study, a number of motor nuclei such as the facial nucleus, the red nucleus, the motor trigeminal nucleus, the substantia nigra and ventral tegmental nuclei expressed MD2. The latter two nuclei showed MD2 dopaminergic neurons projecting to the striatum. These dopaminergic projections are well known for their involvement in regulating movement and sabotaged in Parkinson's disease [49]. This raises the question of what physiological roles MD2 play in movement control of the body, eyes, and the face.

Conclusion

MD2 was found to be primarily expressed by neurons in the brain. It might be involved in diverse neural functions other than mediating neuroinflammation through microglia. Future studies are required to reveal its roles in physiological and pathological conditions.

Abbreviations

3N oculomotor nucleus

4N trochlear nucleus

5N motor trigeminal nucleus

6N abducens nucleus

7N facial nucleus

7SH facial nucleus, stylohyoid part

9Cb lobule 9 of the cerebellar vermis

10N vagus nerve nucleus

12N hypoglossal nucleus

AA anterior amygdaloid area

AcbC accumbens nucleus, core

AcbShaccumbens nucleus, shell

AD anterodorsal thalamic nucleus

AHA anterior hypothalamic area, anterior part

AHC anterior hypothalamic area, central part

AHP anterior hypothalamic area, posterior part

AID agranular insular cortex, dorsal part

AIV agranular insular cortex, ventral part

AM anteronedial thalamic nucleus

Amb ambiguus nucleus

AOD anterior olfactory area, dorsal part

AOL anterior olfactory area, lateral part

AOM anterior olfactory area, medial part

AOV anterior olfactory area, ventral part

AOP anterior olfactory area, posterior part

AP-1 activator protein-1

APT anterior pretectal nucleus

Au1 auditory cortex

AV anteroventral thalamic nucleus

AVPe anteroventral periventricular nucleus

Bar Barrington nucleus

BLA basolateral amygdaloid nucleus, anterior part

BLP basolateral amygdaloid nucleus, posterior part

BMA basomedial amygdaloid nucleus, anterior part

CAT central nucleus of the acoustic tract

CD14 cluster of differentiation 14

CM central medial thalamic nucleus

CPu caudate putamen

CREBcAMP response element binding protein

Cu cuneate nucleus

DAB 3,3,-diaminobenzidine

DEn dorsal endopiriform claustrum

DG dentate gyrus

DI dysgranular insular cortex

Dk nucleus of Darkschewitsch

DLEntdorsolateral entorhinal cortex

DLG dorsal lateral geniculate nucleus

DM dorsomedial hypothalamic nucleus

DP dorsal peduncular cortex

DpG deep gray layer of the superior colliculus

DPGi dorsal paragigantocellular nucleus

DS dorsal subiculum

DTT dorsal tenia tecta

DCl dorsal claustrum

ECu external cuneate nucleus

EP entopedunclular nucleus

F fields of Forel

fr fasciculus retroflexus

FrA frontal association area

g7 genu of the facial nerve

Gi gigantocellular reticular nucleus

GP globus pallidus

HDB horizontal diagonal band

IC inferior colliculus

ICj island of Calleja

IEn intermediate endopiriform claustrum

IL infralimbic cortex

InC interstitial nucleus of Cajal

InG intermediate gray layer of the superior colliculus

IntA interposed cerebellar nucleus, anterior part

IntP interposed cerebellar nucleus, posterior part

IO inferior olive

IP interpeduncular nucleus

IPAC interstitial nucleus of the posterior limb of the anterior commissure

IRt intermediate reticular nucleus

Lat lateral cerebellar nucleus

LBP lipopolysaccharide binding protein

LC locus coeruleus

LDDM laterodorsal thalamic nucleus, dorsomedial part

LDTglaterodorsal tegmental nucleus

LH lateral hypothalamus

Li linear nucleus

LO lateral orbital cortex

LPB lateral parabrachial nucleus

LPO lateral preoptic area

LPS lipopolysaccharide

LRt lateral reticular nucleus

LSD lateral septum, dorsal part

LSI lateral septum, intermediate part

LSV lateral septum, ventral part

Lth lithoid nucleus

LVe lateral vestibular nucleus

M1 primary motor cortex

M2 secondary motor cortex

MAPKmitogen-activated protein kinase

MCLHmagnocellular nucleus of the lateral hypothalamus

MCPCmagnocellular nucleus of the posterior commissure

MD2 Myeloid differentiation factor 2

MdD dorsal medullary reticular nucleus

MdV ventral medullary reticular nucleus

Med medial cerebellar nucleus

MG medial geniculate

mlf medial longitudinal fasciculus

MnPOmedian preoptic nucleus

MnR median raphe nucleus

MO medial orbital cortex

MPA medial preoptic area

MPB medial parabrachial nucleus

MPO medial preoptic nucleus

mRt mesencephalic reticular formation

MS medial septum

MVe medial vestibular nucleus

MVPOmedioventral periolivary nucleus

Myd88myeloid differentiation primary response 88

NF-kBnuclear factor k-B

OT nucleus of the optic tract

p1Rt reticular formation of prosomere 1

PAG periaqueductal gray

PaAP paraventricular hypothalamic nucleus, anterior parvicellular part

PaMMparaventricular hypothalamic nucleus, medial magnocellular part

PaMPparaventricular hypothalamic nucleus, medial parvicellular part

PaPo paraventricular hypothalamic nucleus, posterior part

PBG parabigeminal nucleus

PC pericentral thalamic nucleus

PCRt parvicellular reticular nucleus

PDTgposterodorsal tegmental nucleus

PF parafascicular thalamic nucleus

Pir piriform cortex

PL paralemniscal nucleus

PLCOposterolateral cortical amygdaloid nucleus

PLH lateral hypothalamus, peduncular part

Pn pontine nuclei

PnO pontine reticular nucleus, oral part

PnC pontine reticular nucleus, caudal part

Pr prepositus nucleus

PR prerubral field

Pr5 principal sensory trigeminal nucleus

Pr5DMprincipal sensory trigeminal nucleus, dorsal medial part

PrCnFprecuneiform nucleus

PrEWpre-Edinger Westphal nucleus

PRh perirhinal cortex

PrL prelimbic cortex

PSTh parasubthalamic nucleus

Re reuniens thalamic nucleus

RMC red nucleus, magnocellular part

RMg raphe magnus nucleus

RPa raphe pallidus nucleus

RPF retroparafascicular nucleus

Rt reticular nucleus

RtTg reticulotegmental nucleus of the pons

S1 primary sensory cortex

SC superior colliculus

SIB substantia innominate, basal part

SNC substantia nigra, compact part

SNR substantia nigra, reticular part

Sp5I spinal trigeminal nucleus, interpolar part

Sp5O spinal trigeminal nucleus, oral part

SpVe spinal vestibular nucleus

STh subthalamic nucleus

STM bed nucleus of the stria terminalis

SubC subcoeruleus nucleus

SuVe superior vestibular nucleus

TAK1transforming growth factorβ-activated kinase 1

TLR4Toll-like receptor 4

TRIF Toll-interleukin-1 receptor domain-containing adapter inducing interferon-β

Tu olfactory tubercle

Tz trapezoid nucleus

V1 visual cortex

VCA ventral cochlear nucleus

VCl ventral claustrum

VDB ventral diagonal band

VeCb vestibulocerebellar nucleus

VL ventrolateral thalamic nucleus

VLL ventral nucleus of the lateral lemniscus

VLO ventrolateral orbital cortex

VM ventromedial thalamic nucleus

VMH ventromedial hypothalamic nucleus

VMPOventromedial preoptic nucleus

VO ventral orbital cortex

VP ventral pallidum

VPL ventral posterolateral thalamic nucleus

VTA ventral tegmental area

VTT ventral tenia tecta

ZID zona incerta, dorsal part

Declarations

Ethics approval

This study was approved by the Animal Research Ethics Committee of Tongji University (approval number TJBH00421401).

Consent for publication

Not applicable.

Availability of data and material

The data for producing this manuscript are available from the corresponding author upon reasonable request.

Competing interests

The authors have no relevant financial or non-financial interests to disclose.

Funding

This work was supported by the Major Program of the National Natural Science Foundation of China (No.82130121) to Dr. Lize Xiong, the grant from the National Natural Science Foundation of China

(No.81974535) to Dr. Huazheng Liang, and the Talent Promotion Program of Shanghai Fourth People's Hospital Affiliated to Tongji University School of Medicine (SY-XKZT-2019-3006) to Dr. Zhen Li.

Author contributions

Huazheng Liang and Lize Xiong contributed to the study conception and design. Material preparation, data collection and analysis were performed by Zhen Li, Qianyu Dong, and Hanxi Wan. The first draft of the manuscript was written by Zhen Li and all authors commented on previous versions of the manuscript. All authors read and approved the final manuscript.

Acknowledgement

Not applicable.

References

1. Garate I, Garcia-Bueno B, Madrigal JL, Bravo L, Berrocoso E, Caso JR, Mico JA, Leza JC. Origin and consequences of brain Toll-like receptor 4 pathway stimulation in an experimental model of depression. J Neuroinflammation. 2011;8:151.
2. MacDowell KS, Caso JR, Martin-Hernandez D, Madrigal JL, Leza JC, Garcia-Bueno B. Paliperidone prevents brain toll-like receptor 4 pathway activation and neuroinflammation in rat models of acute and chronic restraint stress. Int J Neuropsychopharmacol. 2014;18.
3. Miyake K. Roles for accessory molecules in microbial recognition by Toll-like receptors. J Endotoxin Res. 2006;12:195-204.
4. Park BS, Song DH, Kim HM, Choi BS, Lee H, Lee JO. The structural basis of lipopolysaccharide recognition by the TLR4-MD-2 complex. Nature. 2009;458:1191-1195.
5. Buchanan MM, Hutchinson M, Watkins LR, Yin H. Toll-like receptor 4 in CNS pathologies. J Neurochem. 2010;114:13-27.
6. Vaure C, Liu Y. A comparative review of toll-like receptor 4 expression and functionality in different animal species. Front Immunol. 2014;5:316.
7. Akira S, Takeda K. Toll-like receptor signalling. Nat Rev Immunol. 2004;4:499-511.
8. Rehman SU, Ali T, Alam SI, Ullah R, Zeb A, Lee KW, Rutten BPF, Kim MO. Ferulic Acid Rescues LPS-Induced Neurotoxicity via Modulation of the TLR4 Receptor in the Mouse Hippocampus. Mol Neurobiol. 2019;56:2774-2790.
9. Zusso M, Lunardi V, Franceschini D, Pagetta A, Lo R, Stifani S, Frigo AC, Giusti P, Moro S. Ciprofloxacin and levofloxacin attenuate microglia inflammatory response via TLR4/NF-kB pathway. J Neuroinflammation. 2019;16:148.

10. Manicassamy S, Pulendran B. Dendritic cell control of tolerogenic responses. Immunol Rev. 2011;241:206-227.
11. Saavedra JM. Angiotensin II AT(1) receptor blockers as treatments for inflammatory brain disorders. Clin Sci (Lond). 2012;123:567-590.
12. Wardill HR, Van Sebille YZ, Mander KA, Gibson RJ, Logan RM, Bowen JM, Sonis ST. Toll-like receptor 4 signaling: a common biological mechanism of regimen-related toxicities: an emerging hypothesis for neuropathy and gastrointestinal toxicity. Cancer Treat Rev. 2015;41:122-128.
13. O'Neill LA, Bowie AG. The family of five: TIR-domain-containing adaptors in Toll-like receptor signalling. Nat Rev Immunol. 2007;7:353-364.
14. Lehnardt S, Massillon L, Follett P, Jensen FE, Ratan R, Rosenberg PA, Volpe JJ, Vartanian T. Activation of innate immunity in the CNS triggers neurodegeneration through a Toll-like receptor 4-dependent pathway. Proc Natl Acad Sci U S A. 2003;100:8514-8519.
15. Gaikwad S, Agrawal-Rajput R. Lipopolysaccharide from Rhodobacter sphaeroides Attenuates Microglia-Mediated Inflammation and Phagocytosis and Directs Regulatory T Cell Response. Int J Inflam. 2015;2015:361326.
16. Trotta T, Porro C, Calvello R, Panaro MA. Biological role of Toll-like receptor-4 in the brain. J Neuroimmunol. 2014;268:1-12.
17. Shabab T, Khanabdali R, Moghadamtousi SZ, Kadir HA, Mohan G. Neuroinflammation pathways: a general review. Int J Neurosci. 2017;127:624-633.
18. Peng Y, Zhang X, Zhang T, Grace PM, Li H, Wang Y, Li H, Chen H, Watkins LR, Hutchinson MR, Yin H, Wang X. Lovastatin inhibits Toll-like receptor 4 signaling in microglia by targeting its co-receptor myeloid differentiation protein 2 and attenuates neuropathic pain. Brain Behav Immun. 2019;82:432-444.
19. D'Agostino PM, Gottfried-Blackmore A, Anandasabapathy N, Bulloch K. Brain dendritic cells: biology and pathology. Acta Neuropathol. 2012;124:599-614.
20. De Laere M, Berneman ZN, Cools N. To the Brain and Back: Migratory Paths of Dendritic Cells in Multiple Sclerosis. J Neuropathol Exp Neurol. 2018;77:178-192.
21. Olson JK, Miller SD. Microglia initiate central nervous system innate and adaptive immune responses through multiple TLRs. J Immunol. 2004;173:3916-3924.
22. Bowman CC, Rasley A, Tranguch SL, Marriott I. Cultured astrocytes express toll-like receptors for bacterial products. Glia. 2003;43:281-291.
23. Wadachi R, Hargreaves KM. Trigeminal nociceptors express TLR-4 and CD14: a mechanism for pain due to infection. J Dent Res. 2006;85:49-53.
24. Bsibsi M, Ravid R, Gveric D, van Noort JM. Broad expression of Toll-like receptors in the human central nervous system. J Neuropathol Exp Neurol. 2002;61:1013-1021.
25. Fenton MJ, Golenbock DT. LPS-binding proteins and receptors. J Leukoc Biol. 1998;64:25-32.

26. Ranoa DRE, Kelley SL, Tapping RI. Human lipopolysaccharide-binding protein (LBP) and CD14 independently deliver triacylated lipoproteins to Toll-like receptor 1 (TLR1) and TLR2 and enhance formation of the ternary signaling complex. J Biol Chem. 2013;288:9729-9741.
27. Fang ZP, Wu D, J. D, Yang QZ, Zhang XJ, Chen J, Wang SQ, Hu SJ, Hou WG, Ning SM, Ding Y, Fan ZM, Jiang ZH, Kang JJ, Liu YY, Miao JL, Ji XM, Dong HL, Xiong LZ. An MD2-perturbing peptide has therapeutic effects in rodent and rhesus monkey models of stroke. Sci Transl Med. 2021;13:eabb6716.
28. George Paxinos, Franklin KBJ. The Mouse Brain in Stereotaxic Coordinates. Fourth edn. (Elsevier Academic Press; 2013).
29. Kunda PE, Cavicchia JC, Acosta CG. Lipopolysaccharides and trophic factors regulate the LPS receptor complex in nodose and trigeminal neurons. Neuroscience. 2014;280:60-72.
30. Zuo W, Zhao J, Zhang J, Fang Z, Deng J, Fan Z, Guo Y, Han J, Hou W, Dong H, Xu F, Xiong L. MD2 contributes to the pathogenesis of perioperative neurocognitive disorder via the regulation of alpha5GABAA receptors in aged mice. J Neuroinflammation. 2021;18:204.
31. Shimazu R, Akashi S, Ogata H, Nagai Y, Fukudome K, Miyake K, Kimoto M. MD-2, a molecule that confers lipopolysaccharide responsiveness on Toll-like receptor 4. J Exp Med. 1999;189:1777-1782.
32. Walter S, Letiember M, Liu Y, Heine H, Penke B, Hao W, Bode B, Manietta N. Role of the Toll-Like Receptor 4 in Neuroinflammation in Alzheimer's Disease. Cell Physiol Biochem. 2007;20:947-956.
33. Liu L, Ghosh N, Slivka PF, Fiorini Z, Hutchinson MR, Watkins LR, Yin H. An MD2 hot-spot-mimicking peptide that suppresses TLR4-mediated inflammatory response in vitro and in vivo. Chembiochem. 2011;12:1827-1831.
34. Park SH, Kyeong MS, Hwang Y, Ryu SY, Han SB, Kim Y. Inhibition of LPS binding to MD-2 co-receptor for suppressing TLR4-mediated expression of inflammatory cytokine by 1-dehydro-10-gingerdione from dietary ginger. Biochem Biophys Res Commun. 2012;419:735-740.
35. Kim MJ, Choi NY, Koo JE, Kim SY, Joung SM, Jeong E, Lee JY. Suppression of Toll-like receptor 4 activation by endogenous oxidized phosphatidylcholine, KOdiA-PC by inhibiting LPS binding to MD2. Inflamm Res. 2013;62:571-580.
36. Kim SY, Koo JE, Seo YJ, Tyagi N, Jeong E, Choi J, Lim KM, Park ZY, Lee JY. Suppression of Toll-like receptor 4 activation by caffeic acid phenethyl ester is mediated by interference of LPS binding to MD2. Br J Pharmacol. 2013;168:1933-1945.
37. Fu W, Chen L, Wang Z, Zhao C, Chen G, Liu X, Dai Y, Cai Y, Li C, Zhou J, Liang G. Determination of the binding mode for anti-inflammatory natural product xanthohumol with myeloid differentiation protein 2. Drug Des Devel Ther. 2016;10:455-463.
38. Zhang Y, Liu Z, Wu J, Bai B, Chen H, Xiao Z, Chen L, Zhao Y, Lum H, Wang Y, Zhang H, Liang G. New MD2 inhibitors derived from curcumin with improved anti-inflammatory activity. Eur J Med Chem. 2018;148:291-305.
39. Gu J, Su S, Guo J, Zhu Y, Zhao M, Duan JA. Anti-inflammatory and anti-apoptotic effects of the combination of Ligusticum chuanxiong and Radix Paeoniae against focal cerebral ischaemia via

TLR4/MyD88/MAPK/NF-kappaB signalling pathway in MCAO rats. J Pharm Pharmacol. 2018;70:268-277.

40. Li M, Liu J, Bi Y, Chen J, Zhao L. Potential Medications or Compounds Acting on Toll-like Receptors in Cerebral Ischemia. Curr Neuropharmacol. 2018;16:160-175.
41. Duan GJ, Zhu J, Xu JH, Liu YS. Targeting myeloid differentiation 2 for treatment of sepsis. Front Biosci. 2014;19:904-915.
42. Wang Y, Shan X, Chen G, Jiang L, Wang Z, Fang Q, Liu X, Wang J, Zhang Y, Wu W, Liang G. MD-2 as the target of a novel small molecule, L6H21, in the attenuation of LPS-induced inflammatory response and sepsis. Br J Pharmacol. 2015;172:4391-4405.
43. Fang Q, Wang L, Yang D, Chen X, Shan X, Zhang Y, Lum H, Wang J, Zhong P, Liang G, Wang Y. Blockade of myeloid differentiation protein 2 prevents obesity-induced inflammation and nephropathy. J Cell Mol Med. 2017;21:3776-3786.
44. Jin J, Yu X, Hu Z, Tang S, Zhong X, Xu J, Shang P, Huang Y, Liu H. Isofraxidin targets the TLR4/MD-2 axis to prevent osteoarthritis development. Food Funct. 2018;9:5641-5652.
45. Zhang Y, Xu T, Pan Z, Ge X, Sun C, Lu C, Chen H, Xiao Z, Zhang B, Dai Y, Liang G. Shikonin inhibits myeloid differentiation protein 2 to prevent LPS-induced acute lung injury. Br J Pharmacol. 2018;175:840-854.
46. Chen H, Zhang Y, Zhang W, Liu H, Sun C, Zhang B, Bai B, Wu D, Xiao Z, Lum H, Zhou J, Chen R, Liang G. Inhibition of myeloid differentiation factor 2 by baicalein protects against acute lung injury. Phytomedicine. 2019;63:152997.
47. Liu Z, Chen L, Yu P, Zhang Y, Fang B, Wu C, Luo W, Chen X, Li C, Liang G. Discovery of 3-(Indol-5-yl)-indazole Derivatives as Novel Myeloid Differentiation Protein 2/Toll-like Receptor 4 Antagonists for Treatment of Acute Lung Injury. J Med Chem. 2019;62:5453-5469.
48. Yang J, Liu R, Lu F, Xu F, Zheng J, Li Z, Cui W, Wang C, Zhang J, Xu S, Zhou W, Wang Q, Chen J, Chen X. Fast Green FCF Attenuates Lipopolysaccharide-Induced Depressive-Like Behavior and Downregulates TLR4/Myd88/NF-kappaB Signal Pathway in the Mouse Hippocampus. Front Pharmacol. 2019;10:501.
49. Wei ZD, Shetty AK. Treating Parkinson's disease by astrocyte reprogramming: Progress and challenges. Sci Adv. 2021;7.

Figures

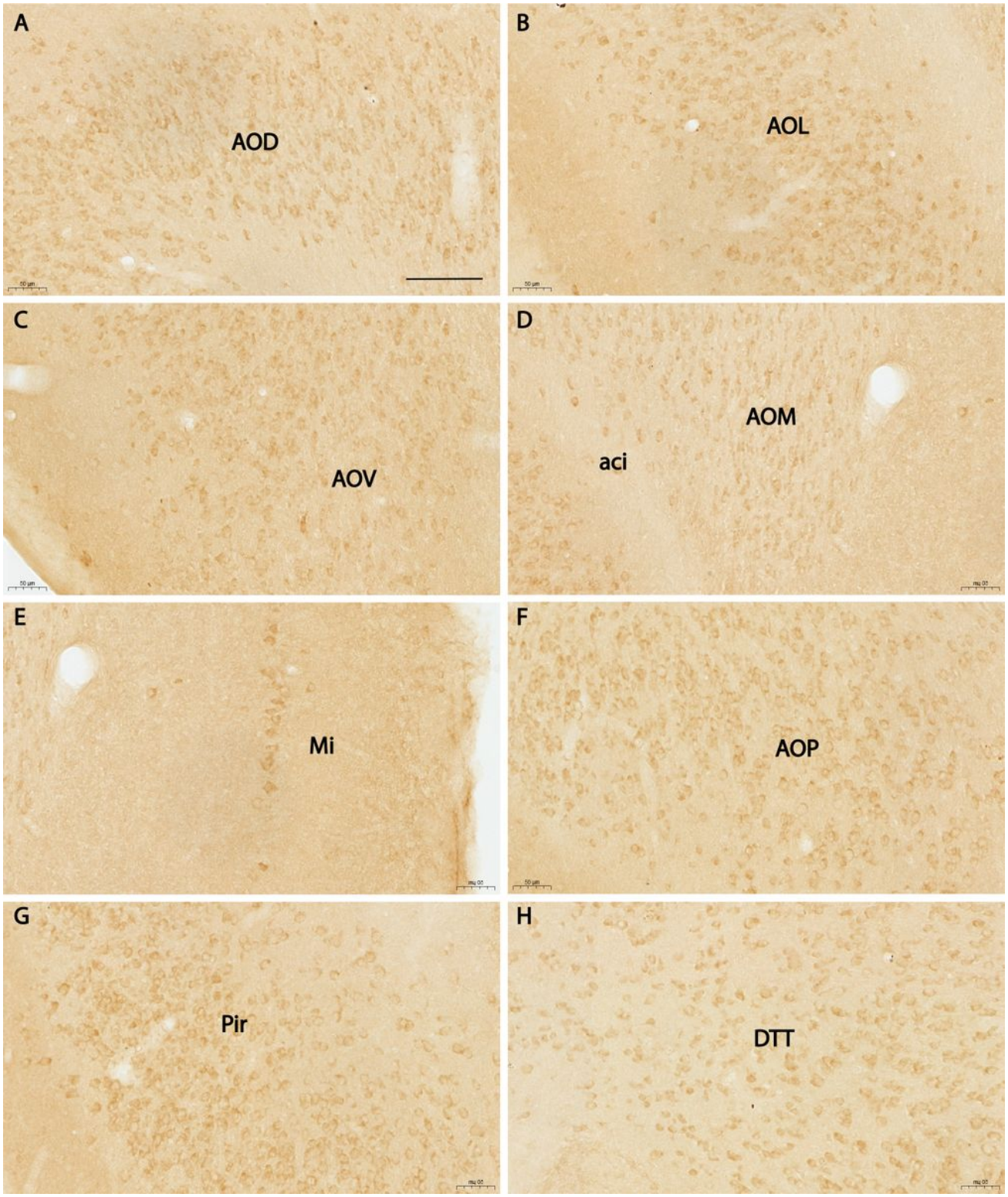

Figure 1

Distribution of MD2 positive cells in the olfactory bulb. **A**. A band of MD2 positive cells in AOD above aci. **B**. A band of MD2 positive cells in AOL lateral to aci. **C**. A cluster of MD2 positive cells in AOV ventral to aci. **D**. MD2 positive cells in AOM medial to aci. **E**. A small number of MD2 positive cells in the mitral cell layer of the olfactory bulb. **F**. A patch of MD2 positive cells in AOP in the caudal part of the olfactory bulb.

G. Densely packed MD2 positive cells in Pir lateral to aci. **H**. MD2 positive cells in DTT of the rostral olfactory bulb. Scale bar = 100 mm.

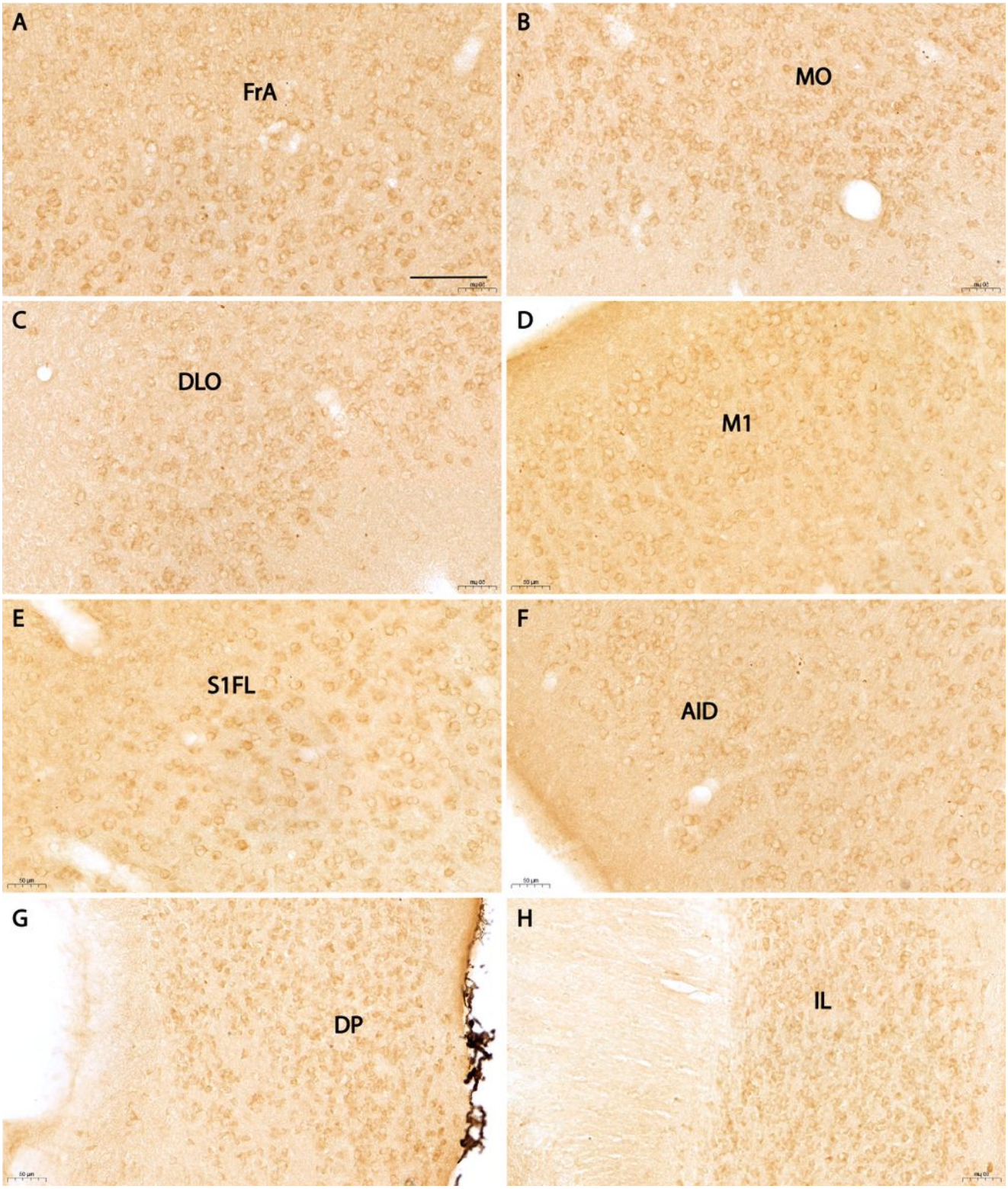

Figure 2

Distribution of MD2 positive cells in the cortex. **A**. MD2 positive cells in FrA in the rostral frontal cortex. **B**. MD2 positive cells in MO dorsal to the olfactory bulb. **C**. MD2 positive cells in DLO dorsal to the olfactory

bulb. **D**. MD2 positive cells in M1. **E**. MD2 positive cells in S1FL. **F**. MD2 positive cells in AID. **G**. Densely packed MD2 positive cells in DP. **H**. MD2 positive cells in IL. Note positive signals were dominantly seen on the membrane. Scale bar = 100 mm.

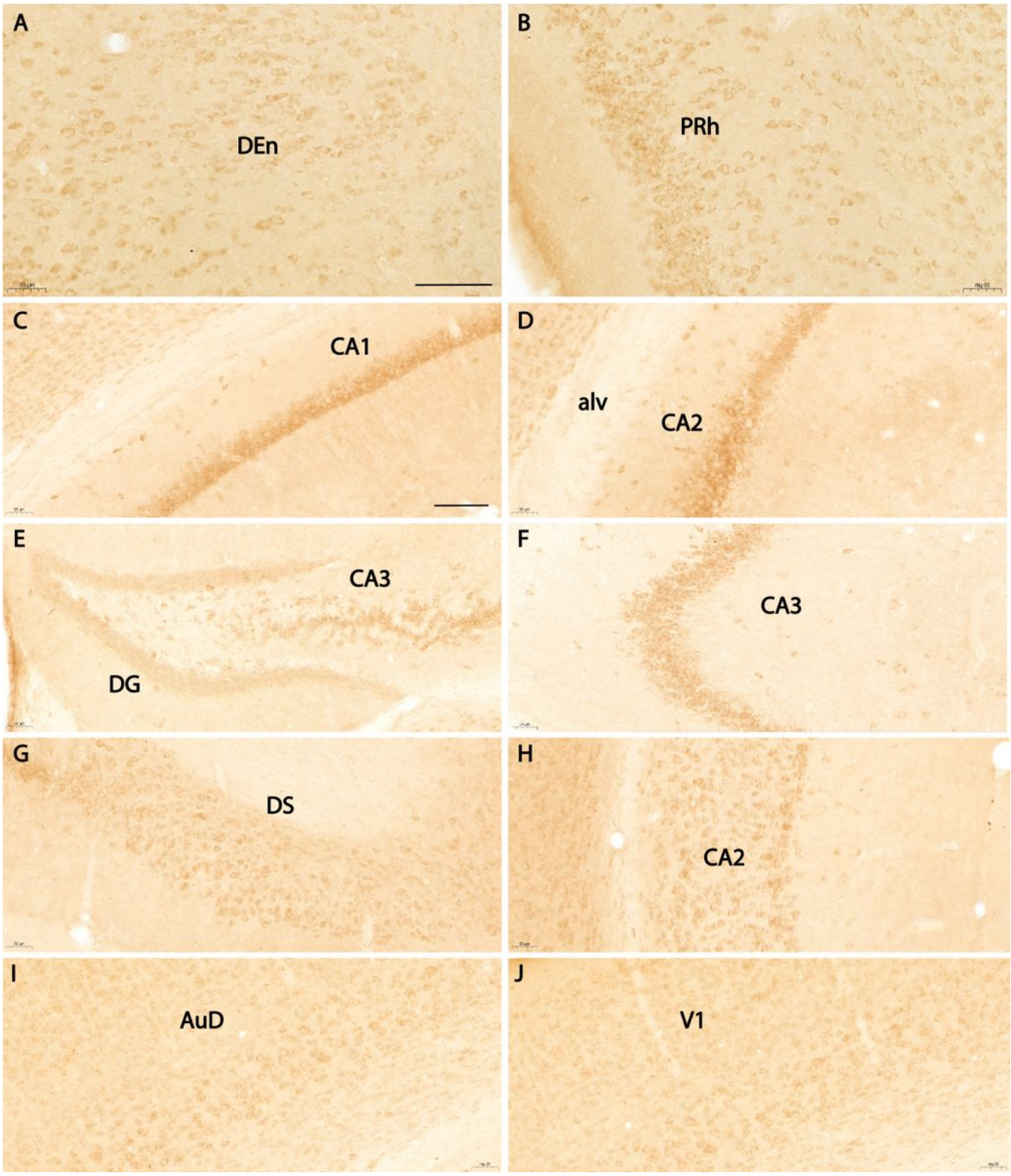

Figure 3

Distribution of MD2 positive cells in the cortex and the hippocampus. **A**. MD2 positive cells in DEn. **B**. MD2 positive cells in PRh. **C**. MD2 positive cells in rostral CA1 of the hippocampus. **D**. MD2 positive cells in rostral CA2 of the hippocampus. **E**. MD2 positive cells in rostral DG and CA3 of the hippocampus. **F**. MD2 positive cells in the lateral part of CA3. Note positive cells in the pyramidal layer. **G**. MD2 positive cells in DS of the caudal hippocampus. **H**. MD2 positive cells in CA2 of the caudal hippocampus. Note positive cells in not only the pyramidal layer, but also other layers. **I**. MD2 positive cells in AuD. Note positive cells mainly in the deep layer. **J**. MD2 positive cells in V1. Note positive cells mainly in the deep layer with few cells in the superficial layers. Scale bar = 100 mm.

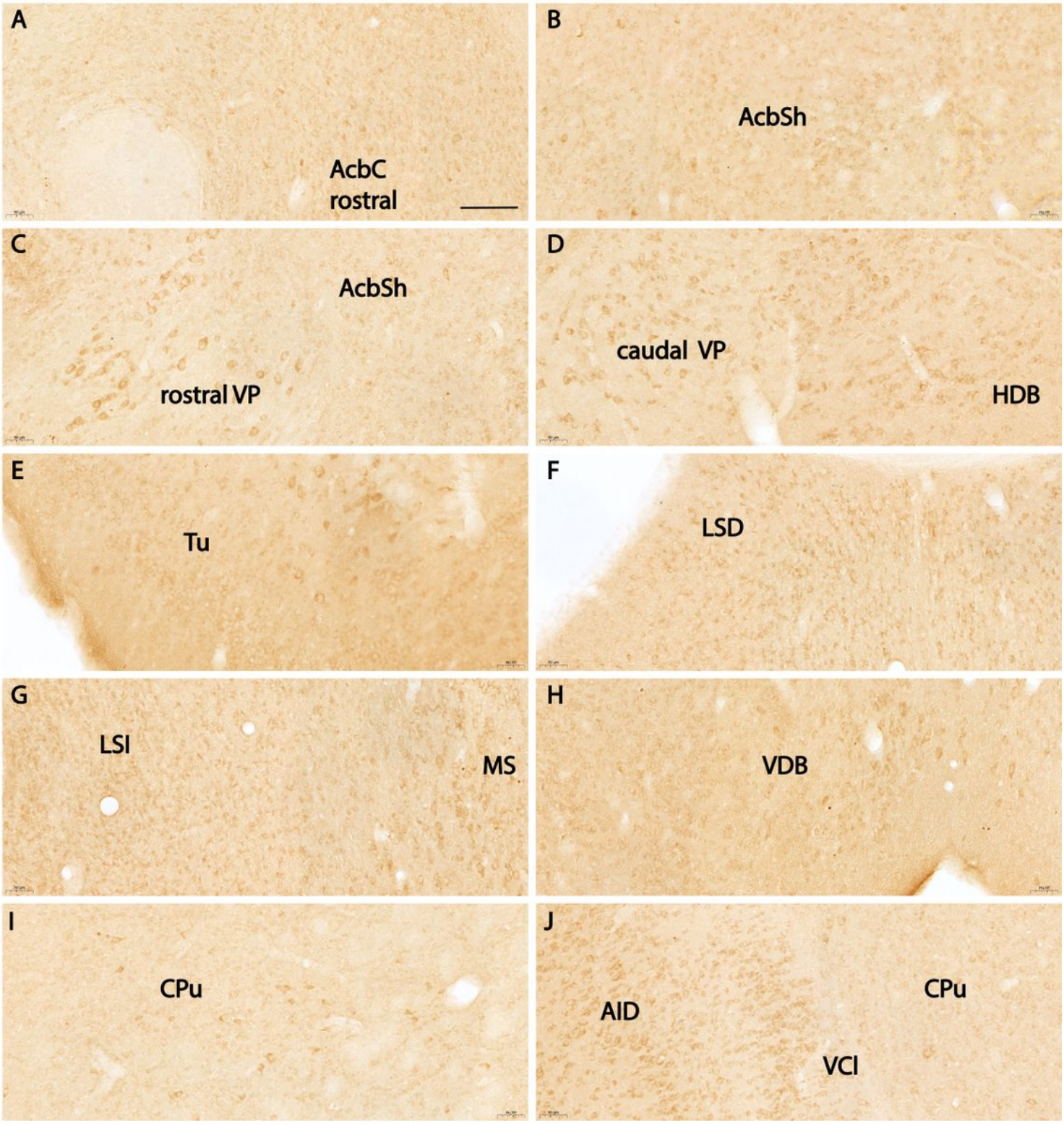

Figure 4

Distribution of MD2 positive cells in subcortical nuclei of the forebrain. **A**. MD2 positive cells in AcbC dorsal to the anterior commissure. **B**. MD2 positive cells in AcbSh ventral to the anterior commissure. **C**. MD2 positive cells in rostral VP. **D**. MD2 positive cells in caudal VP. **E**. MD2 positive cells in Tu. **F**. MD2 positive cells in LSD. **G**. MD2 positive cells in LSI and MS. Note positive cells in MS are more prominent than those in LSD and LSI. **H**. MD2 positive cells in VDB. **I**. MD2 positive cells in CPu. **J**. MD2 positive

cells in VCl. Positive cells in VCl are similar to those in AID and more outstanding than those in CPu. Scale bar = 100 mm.

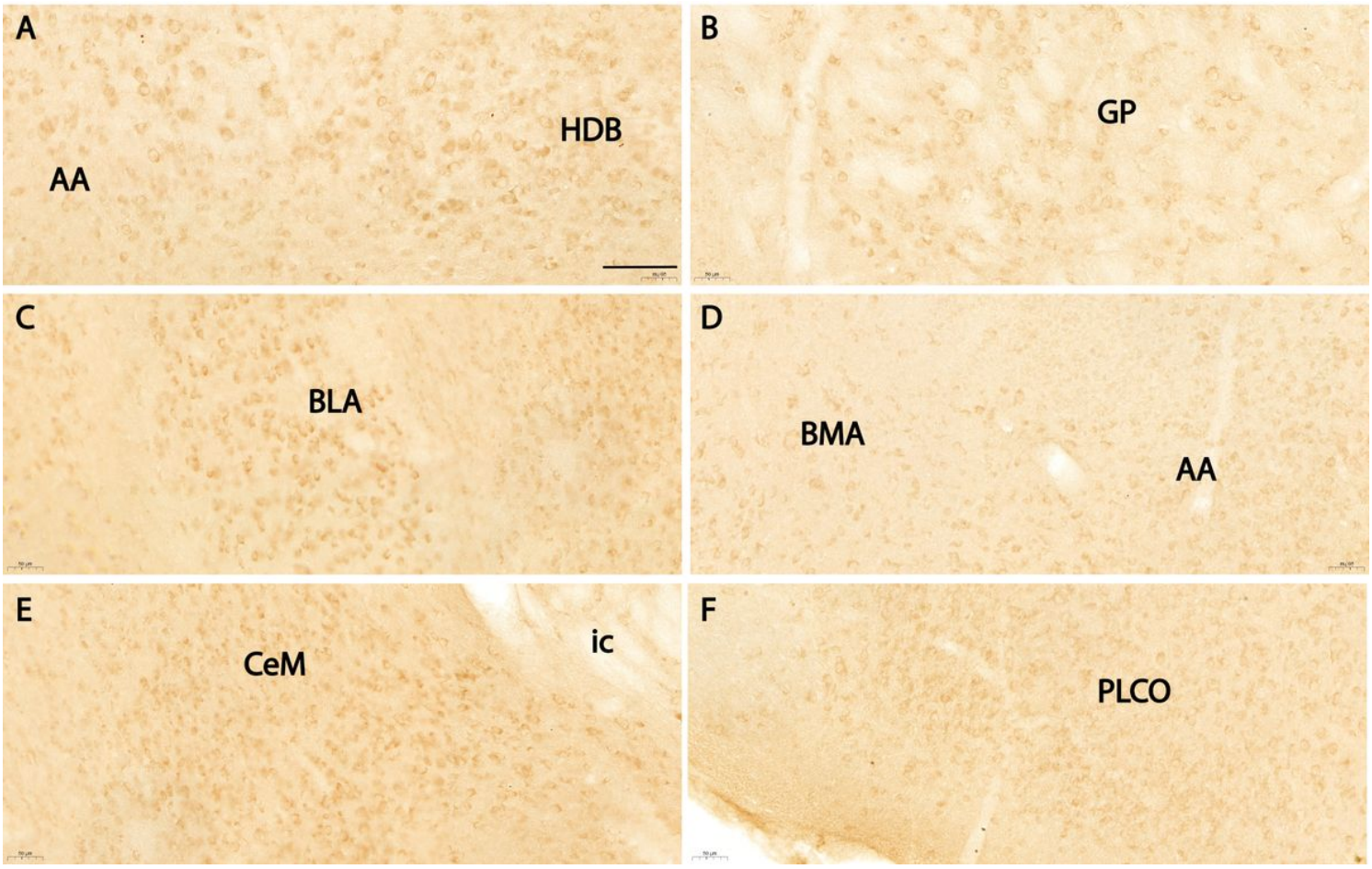

Figure 5

Distribution of MD2 positive cells in subcortical nuclei of the forebrain-continued. **A**. MD2 positive cells in AA. **B**. MD2 positive cells in GP. **C**. MD2 positive cells in rostral BLA. **D**. MD2 positive cells in BMA. **E**. MD2 positive cells in CeM. **F**. MD2 positive cells in PLCO. Note positive cells in AA and BMA are not densely packed like those in BLA and CeM. Scale bar = 100 mm.

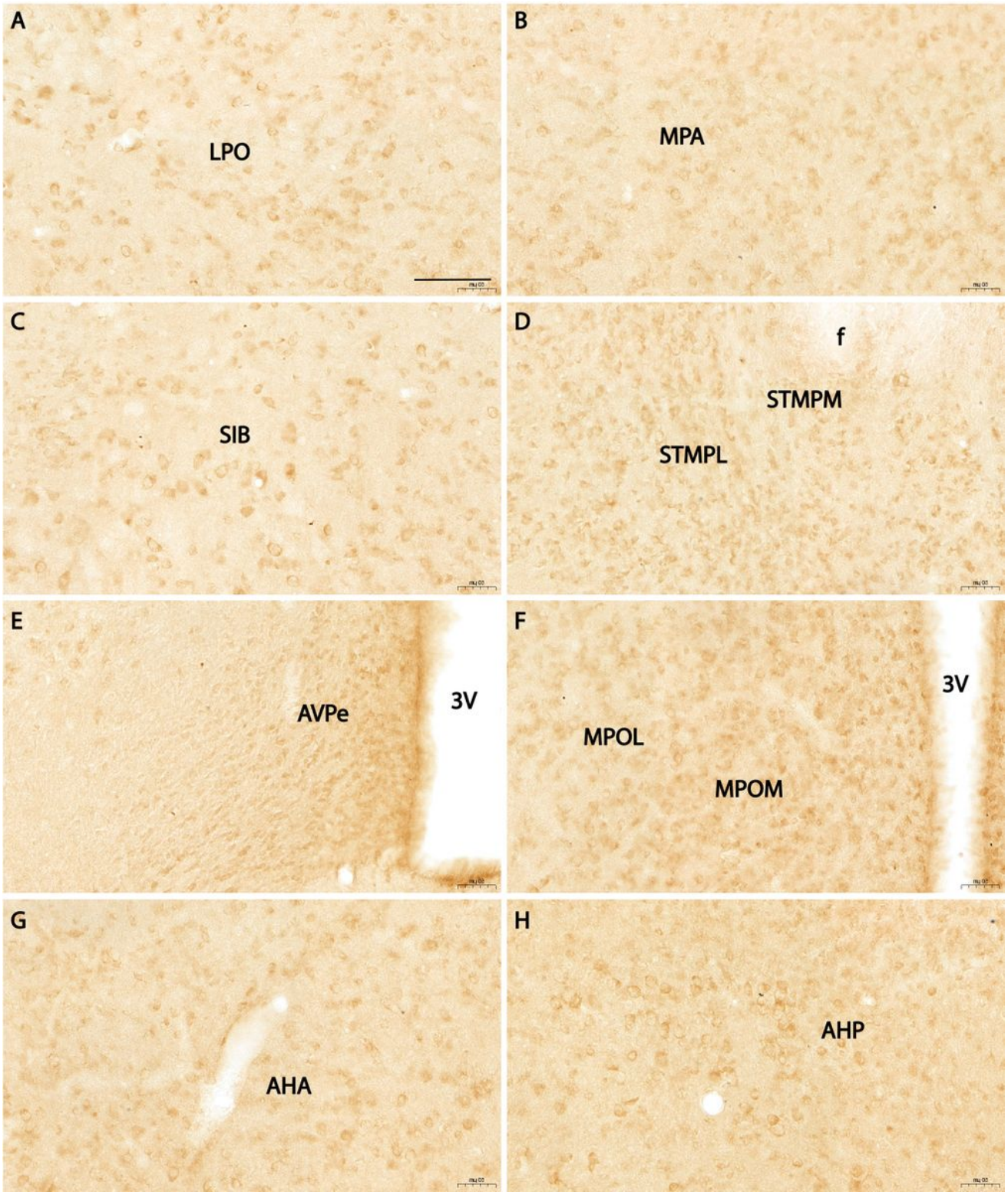

Figure 6

Distribution of MD2 positive cells in the hypothalamus. **A**. MD2 positive cells in rostral LPO. **B**. MD2 positive cells in rostral MPA. **C**. MD2 positive cells in SIB. Note positive cells in these nuclei are similar to each other. **D**. MD2 positive cells in STM including the medial and the lateral nuclei. **E**. MD2 positive cells in rostral AVPe. **F**. MD2 positive cells in MPO including the medial and lateral nuclei. **G**. MD2 positive cells

in AHA. **H**. MD2 positive cells in AHP. Positive cells in AHA and AHP are larger than those in AVPe and MPO. Scale bar = 100 mm.

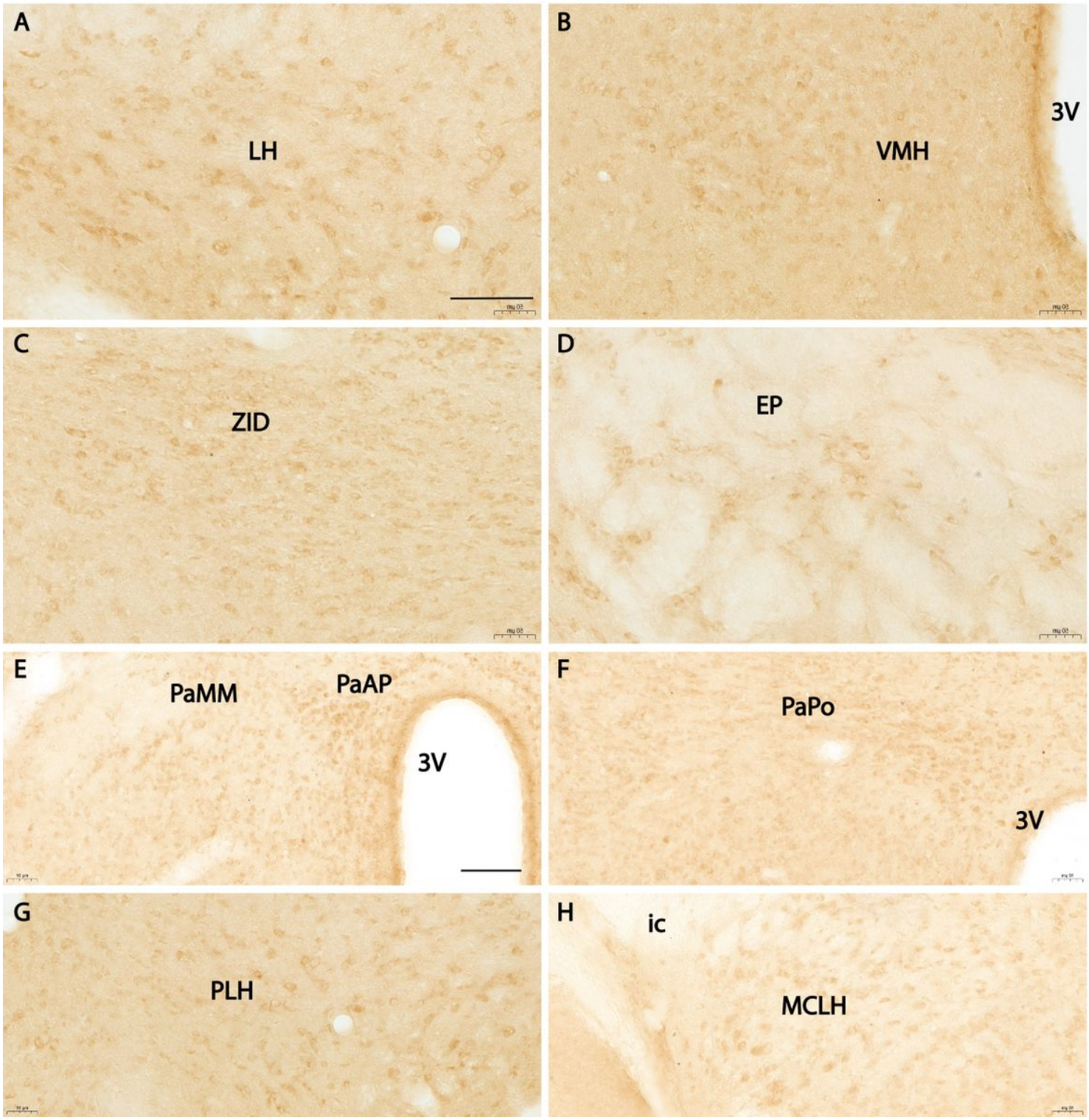

Figure 7

Distribution of MD2 positive cells in the hypothalamus-continued. **A**. MD2 positive cells in LH. **B**. MD2 positive cells in VMH. **C**. MD2 positive cells in rostral ZID. **D**. MD2 positive cells in EP. These cells are similar to those in CPu. **E**. MD2 positive cells in rostral PaAP and PaMM. **F**. MD2 positive cells in PaPo.

These cells are similar to those in PaAP. PaMM has a lower density of positive cells. **G**. MD2 positive cells in PLH. **H**. MD2 positive cells in MCLH. Scale bar = 100 mm.

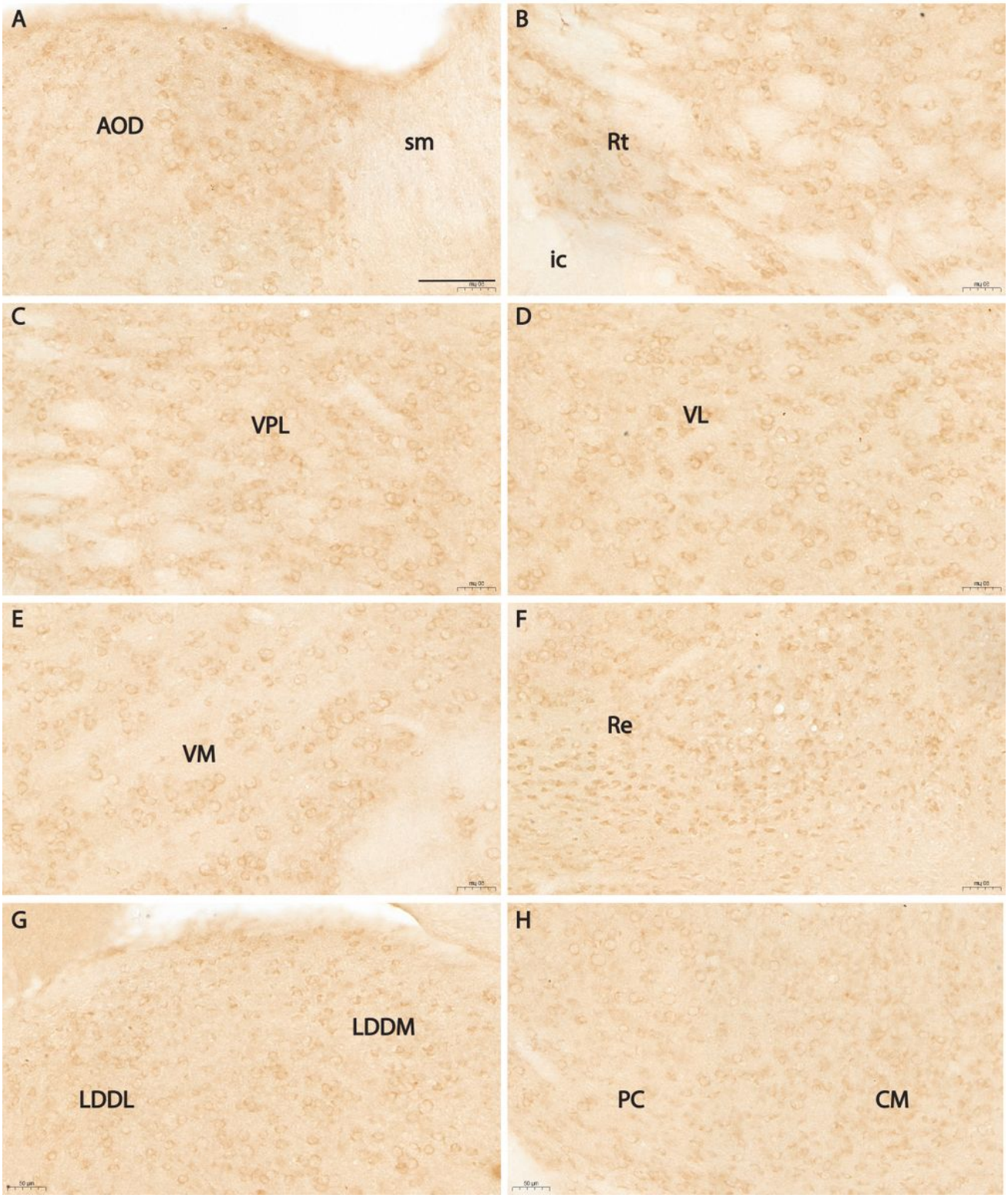

Figure 8

Distribution of MD2 positive cells in the thalamus. **A**. MD2 positive cells in AOD. **B**. MD2 positive cells in Rt. **C**. MD2 positive cells in VPL. **D**. MD2 positive cells in VL. **E**. MD2 positive cells in VM. **F**. MD2 positive

cells in Re. **G**. MD2 positive cells in LDDL and LDDM. **H**. MD2 positive cells in PC and CM. Positive cells are similar in the thalamic nuclei except Re and adjacent nuclei which have smaller positive cells. Scale bar = 100 mm.

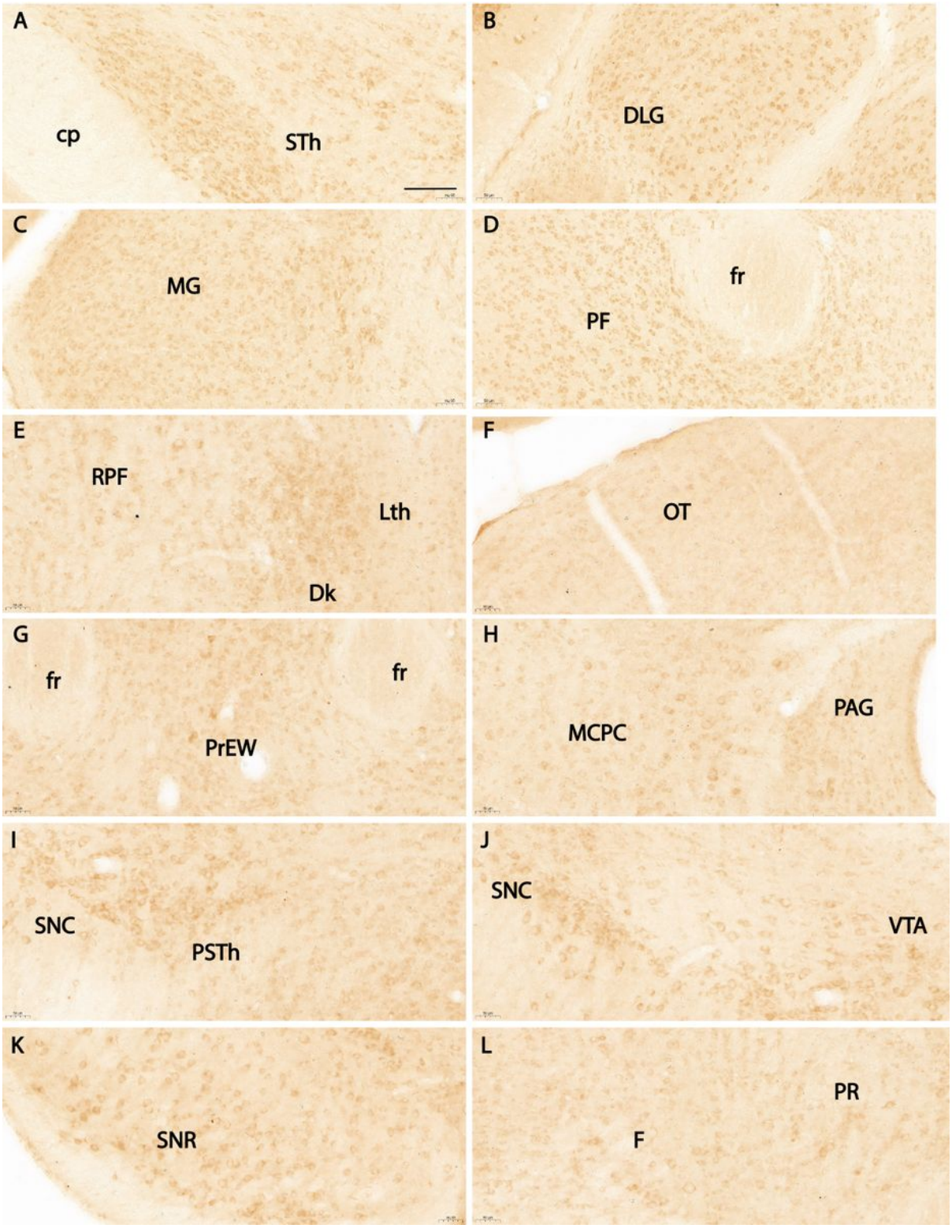

Figure 9

Distribution of MD2 positive cells in the thalamus and pretectum. **A**. MD2 positive cells in STh. **B**. MD2 positive cells in DLG. **C**. MD2 positive cells in MG. **D**. MD2 positive cells in PF. **E**. MD2 positive cells in Lth, Dk, and RPF. **F**. MD2 positive cells in OT. Few positive cells are present in this nucleus. **G**. MD2 positive cells in PrEW. **H**. MD2 positive cells in MCPC and rostral PAG. Note positive cells in MCPC are more prominent than those in PAG. **I**. MD2 positive cells in rostral SNC and PSTh. **J**. MD2 positive cells in SNC and VTA. **K**. MD2 positive cells in SNR. **L**. MD2 positive cells in PR and F. Positive cells in SNC, SNR, and VTA are similar to each other. Scale bar = 100 mm.

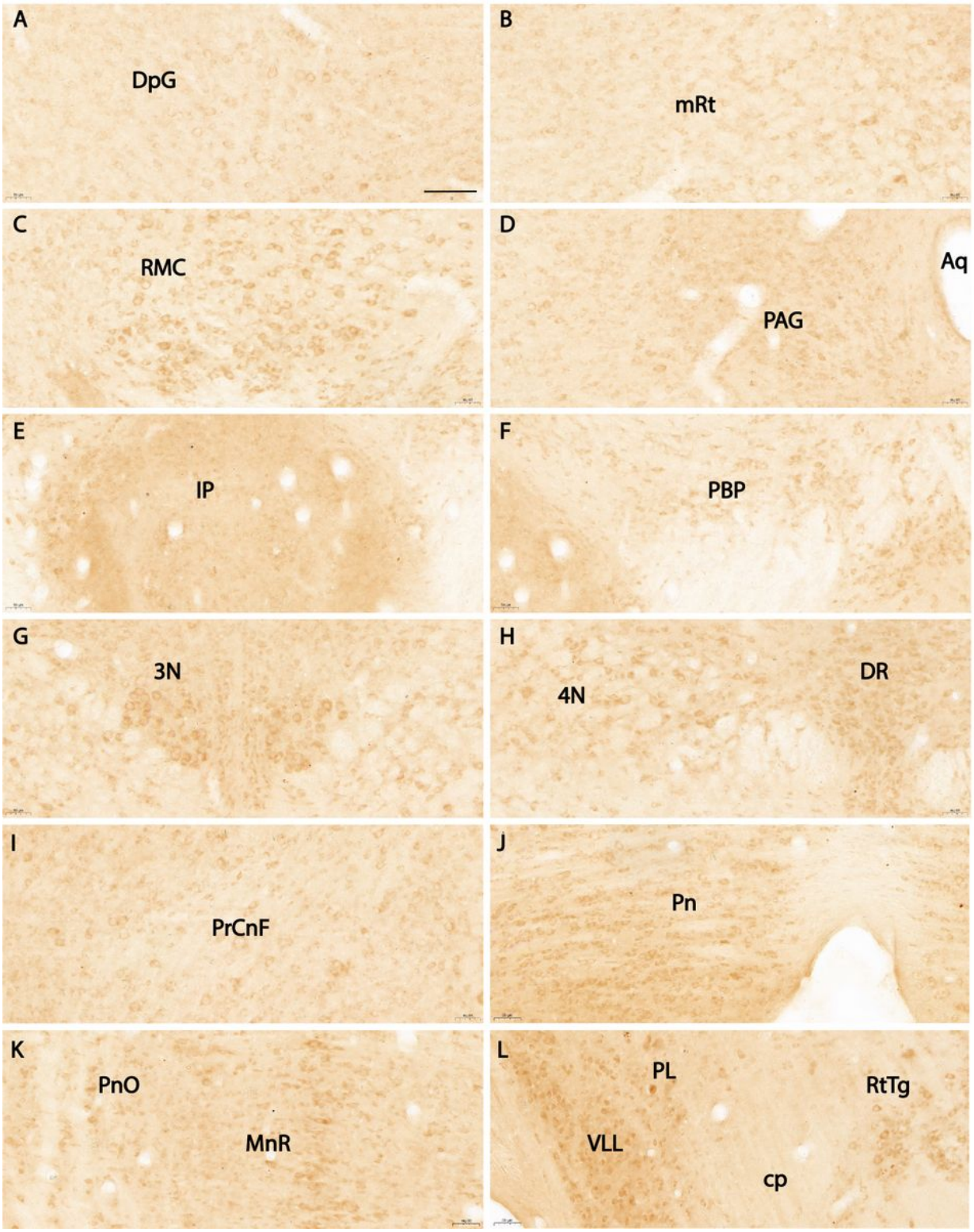

Figure 10

Distribution of MD2 positive cells in the brainstem. **A**. MD2 positive cells in DpG. **B**. MD2 positive cells in mRt. **C**. MD2 positive cells in RMC. **D**. MD2 positive cells in PAG of the midbrain. **E**. MD2 positive cells in IP. Note positive cells in the lateral margin of the nucleus. **F**. MD2 positive cells in PBP. **G**. MD2 positive cells in 3N. **H**. MD2 positive cells in 4N and adjacent DR. **I**. MD2 positive cells in PrCnF which is lateral to PAG and ventral to IC. **J**. MD2 positive cells in pontine nuclei. **K**. MD2 positive cells in MnR and PnO. **L**. MD2 positive cells in VLL, PL and RtTg. Positive cells in Pn are similar to those in RtTg. Scale bar = 100 mm.

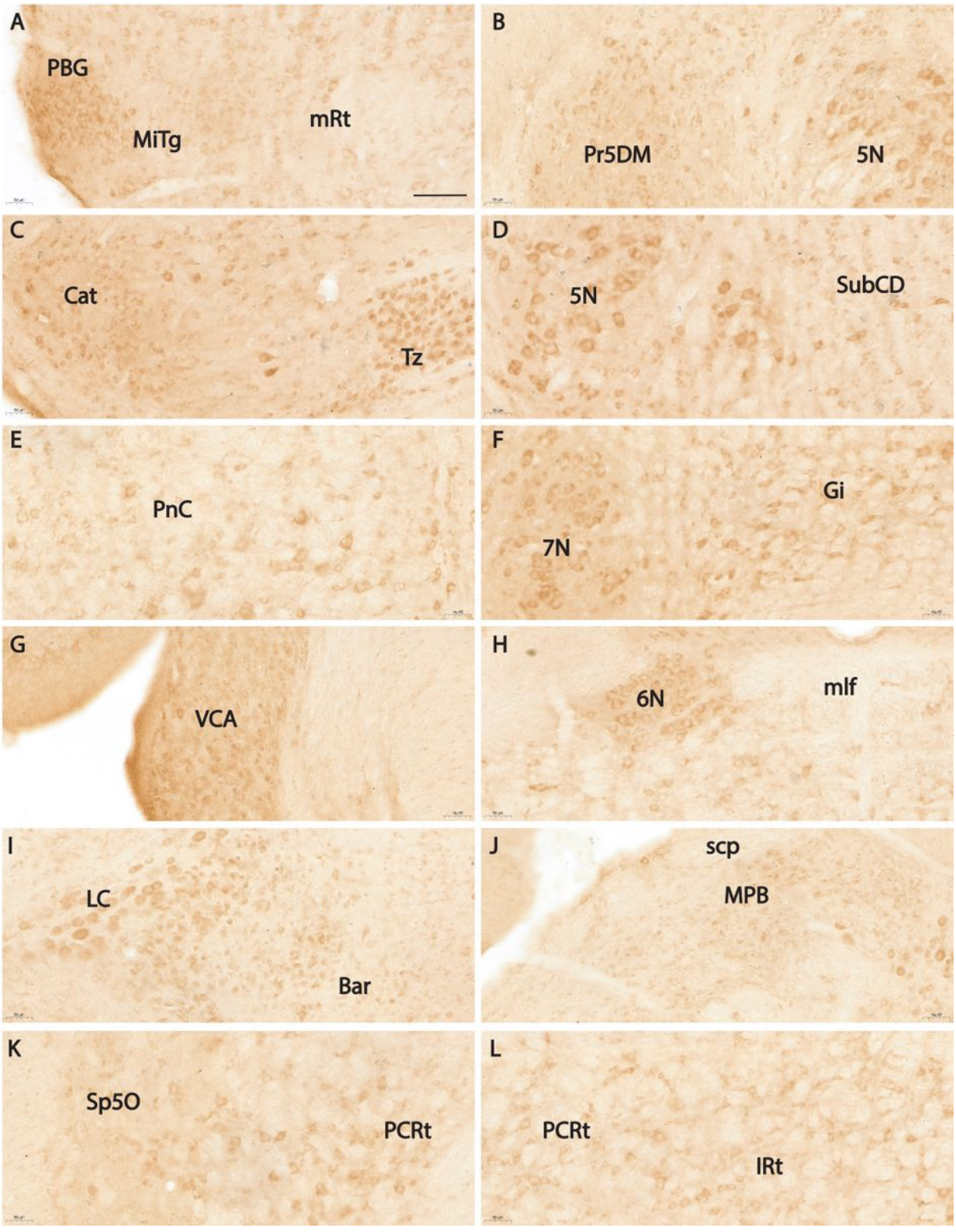

Figure 11

Distribution of MD2 positive cells in the brainstem-continued. **A**. MD2 positive cells in PBG and MiTg. **B**. MD2 positive cells in 5N and Pr5DM. **C**. MD2 positive cells in Tz and CAT. **D**. MD2 positive cells in 5N and SubCD. **E**. MD2 positive cells in PnC. **F**. MD2 positive cells in 7N and Gi. **G**. MD2 positive cells in VCA. **H**. MD2 positive cells in 6N and adjacent reticular formation. **I**. MD2 positive cells in LC and Bar. **J**. MD2 positive cells in MPB. **K**. MD2 positive cells in Sp5O and PCRt. **L**. MD2 positive cells in PCRt and IRt. Note

Positive cells in cranial nuclei are more prominent than those in other nuclei, even the reticular nuclei. Scale bar = 100 mm.

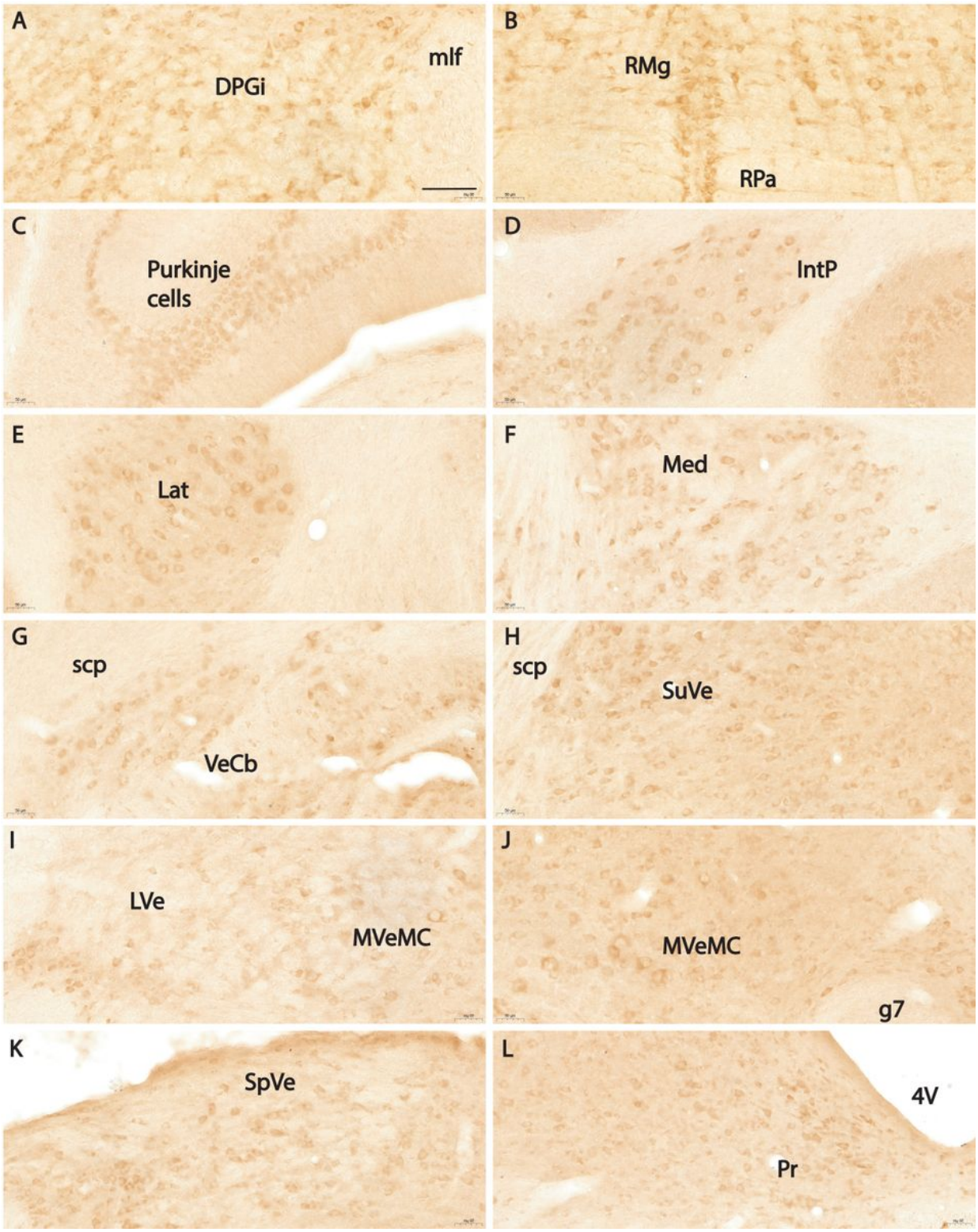

Figure 12

Distribution of MD2 positive cells in the brainstem-continued. **A**. MD2 positive cells in DPGi. **B**. MD2 positive cells in RMg and RPa. **C**. MD2 positive cells in Purkinje cells of the cerebellum. **D**. MD2 positive

cells in IntP. **E**. MD2 positive cells in Lat. **F**. MD2 positive cells in Med. **G**. MD2 positive cells in VeCb. **H**. MD2 positive cells in SuVe. **I**. MD2 positive cells in LVe and MVeMC. **J**. MD2 positive cells in rostral MVeMC. **K**. MD2 positive cells in SpVe. **L**. MD2 positive cells in Pr. Note Positive cells in deep cerebellar nuclei are more prominent than those in vestibular nuclei, except the medial vestibular nucleus. Scale bar = 100 mm.

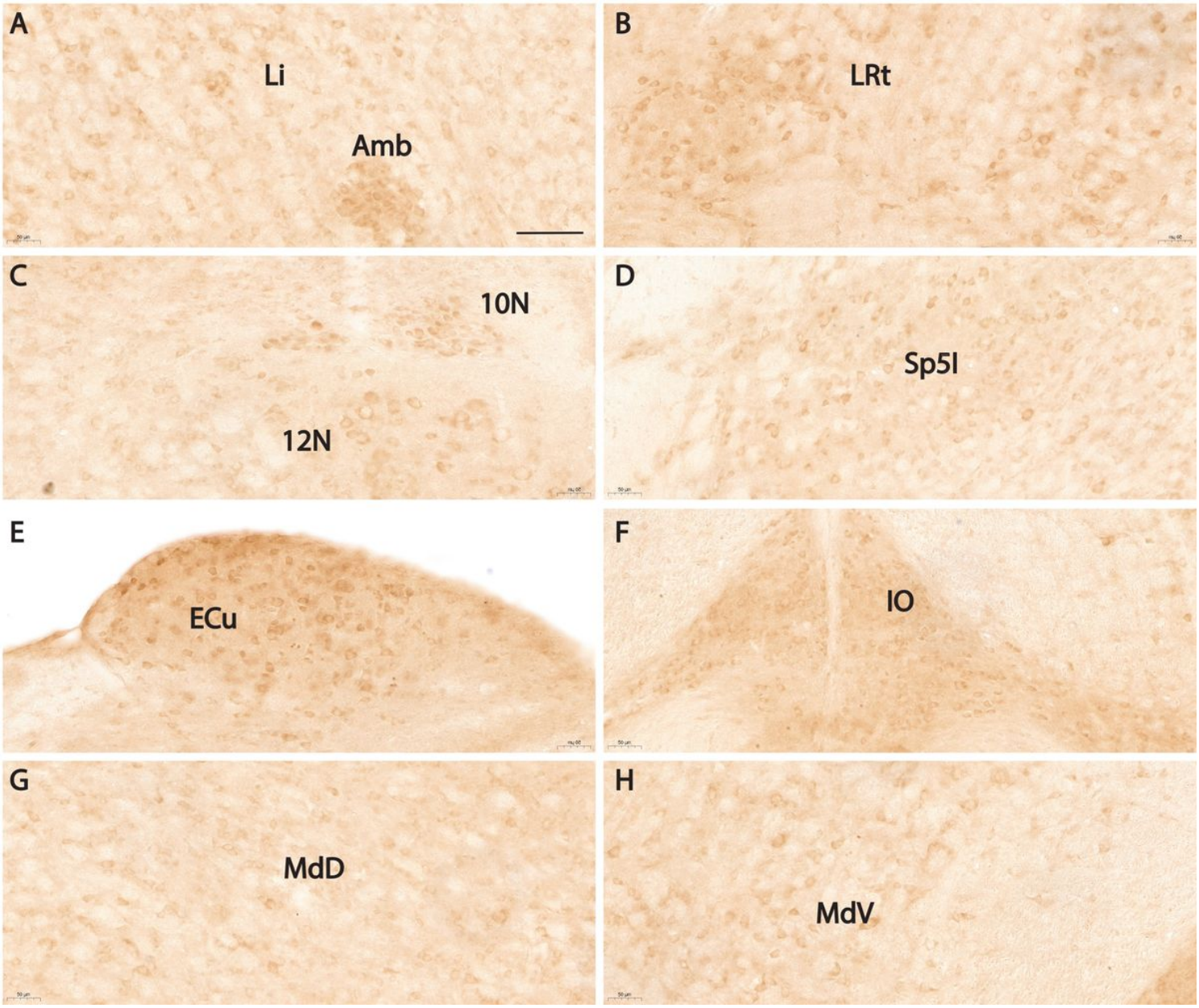

Figure 13

Distribution of MD2 positive cells in the brainstem-continued. **A**. MD2 positive cells in Amb and Li which is dorsal and lateral to Amb. **B**. MD2 positive cells in LRt which is continuous with Li caudally. **C**. MD2 positive cells in 12N and 10N. **D**. MD2 positive cells in Sp5I. **E**. MD2 positive cells in ECu. **F**. MD2 positive cells in IO. **G**. MD2 positive cells in MdD. **H**. MD2 positive cells in MdV. Note Positive cells in cranial nuclei and reticular formation are more prominent than those in the inferior olive. Scale bar = 100 mm.

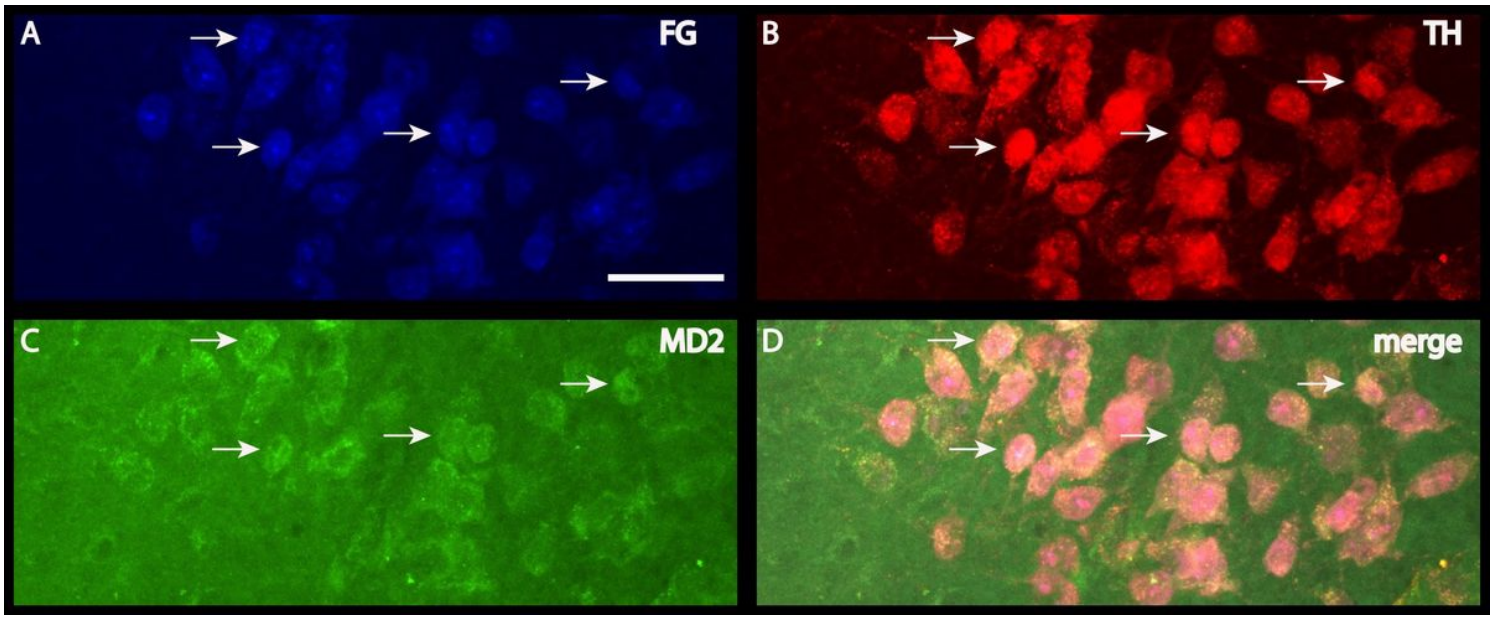

Figure 14

Triple labelling of MD2 positive cells with TH after FG injections into CPu. **A**. FG labelled neurons in the SNC and VTA which is continuous with SNC medially. **B**. TH positive cells in SNC and VTA. **C**. MD2 positive cells in SNC and VTA. **D**. Merge of FG labelled TH and MD2 positive cells in SNC and VTA. Scale bar = 50 mm.